BMC Chemistry

RESEARCH

Open Access

The antibacterial and anti-biofilm effects of novel synthetized nitroimidazole compounds against methicillin-resistant *Staphylococcus aureus* and carbapenem-resistant *Escherichia coli* and *Klebsiella pneumonia* in vitro and in silico

Elham Zarenezhad[1], Esmaeil Behmard[2], Raziyeh Karami[1], Somayeh Behrouz[3], Mahrokh Marzi[1], Abdolmajid Ghasemian[1*] and Mohammad Navid Soltani Rad[3]

Abstract

The antibiotic resistance and biofilm formation by bacterial pathogens has led to failure in infections elimination. This study aimed to assess the antibacterial and anti-biofilm properties of novel synthesized nitroimidazole compounds (**8a–8o**). In this study, nitroimidazole compounds were synthesized via the A3 coupling reaction of sample substrates in the presence of copper-doped silica cuprous sulfate (CDSCS). Fifteen and two carbapenemase producing *Escherichia coli* and *Klebsiella pneumonia* (CP-*E. coli* and CP-*K. pneumonia*, respectively) and one methicillin-resistant *Staphylococcus aureus* (MRSA) and one methicillin-susceptible *S. aureus* (MSSA) plus standard strain of each isolate were included. The antibacterial effects of these compounds demonstrated that the lowest minimum inhibitory and bactericidal concentrations (MIC/MBC, respectively) levels corresponded to compound **8g** against *S. aureus* (1/2 µg/mL) and *K. pneumonia* (8/32 µg/mL) standard and clinical strains and confirmed by in silico assessment. This was comparable to those of metronidazole being 32–128 µg/mL against *K. pneumonia* and 32–64 µg/mL against *S. aureus*. In comparison to metronidazole, against CP-*E. coli*, compounds **8i** and **8m** had significantly higher antibacterial effects ($p < 0.001$) and against CP-*K. pneumonia*, compounds **8a**–**8j** and **8l**–**8o** had significantly higher ($p < 0.0001$) antibacterial effects. Compound **8g** exhibited significantly higher antibacterial effects against MSSA and compounds **8b** ($p < 0.001$), **8c** ($p < 0.001$), **8d** ($p < 0.001$), **8e** ($p < 0.001$) and **8g** ($p < 0.0001$) exerted significantly higher antibacterial effects than metronidazole against MRSA. Moreover, potential anti-biofilm effects was corresponded to compounds **8a**, **8b**, **8c**, **8e**, **8f**, **8g**, **8i**, **8k**, **8m** and **8n**. Considering the antibacterial and anti-biofilm effects of novel synthesized compounds evaluated in this study, further assessments is warranted to verify their properties in vivo and clinical trials in the future.

Keywords Antibiotic resistance, Biofilms, Methicillin-resistant *Staphylococcus aureus*, Carbapenem resistance, Nitroimidazole compounds

*Correspondence:
Abdolmajid Ghasemian
majidghasemian86@gmail.com
Full list of author information is available at the end of the article

Introduction

Antibiotic resistance is a growing global health threat resulting in increased morbidity, mortality and healthcare costs [1, 2]. According to the World Health Organization (WHO), antibiotic resistance is a current leading global threat to health, food security, and development. The indiscriminate and uncontrolled consumption of antibiotics and long-term hospital residence include the primary drivers of antibiotic resistance [3–5]. In these conditions of antibiotics frequent or incorrect utilization, bacterial strains develop various mechanisms of resistance [6, 7]. This also leads to failure in infections eradication, longer hospital stays and higher healthcare costs [8, 9]. If current trends continue, this number could rise to millions of deaths annually by 2050 [10, 11] and pose cost to the global economy up to $100 trillion by 2050 which includes costs associated with increased healthcare spending, lost productivity, and premature death [12, 13]. Carbapenemases are enzymes produced by those Gram-negative bacteria exhibiting resistance to carbapenems via hydrolyzing their β-lactam rings [14, 15]. *Enterobacteriaceae* family members such as *Escherichia coli* (*E. coli*) and *Klebsiella pneumoniae* (*K. pneumoniae*) are among species with this ability causing serious infections such as urinary tract, bloodstream, and gastrointestinal infections and pneumonia [16–18]. Carbapenem-resistant *Enterobacteriaceae* (CRE) are a significant public health threat due to vast resistance phenotype [19–21]. Considering these problems, the development of novel antibiotics, accurate infection prevention and control measures, surveillance to monitor the prevalence and spread of carbapenemase-bearing strains and the appropriate utilization of antibiotics are crucial [22, 23].

Staphylococcus aureus (*S. aureus*) is a ubiquitous bacterium among which MRSA (Methicillin-resistant *Staphylococcus aureus*) strains have acquired a novel penicillin-binding protein (PBP) known as PBP-2a [24]. These strains have developed resistance to several antibiotics, including methicillin and other beta-lactam antibiotics [25–28].

One of the most important bioactive *N*-heterocyles for drug discovery are imidazole compounds and especially nitroimidazole derivatives (NIM). 5-nitroimidazole derivatives [29] including metronidazole (2-Methyl-5-nitroimidazole-1-ethanol), ornidazole (α-(Chloromethyl)-2-methyl-5-nitroimidazole-1-ethanol) and tinidazole (1-[2-(Ethylsulfonyl) ethyl]-2-methyl-5-imidazole) [30] are widely utilized to control diseases caused by protozoan and anaerobic bacterial infections (Fig. 1). Also, 2-methyl-5-nitroimidazole derivatives have been used as antibacterial factors for a long time due to their therapeutic effect [31]. Antimicrobial effects of imidazole, oxadiazole, benzimidazole and thiazole-based schiff containing compounds have been also demonstrated [32–35]. However, nitroheterocyclic compounds have other biological activities [30] like antituberculosis and

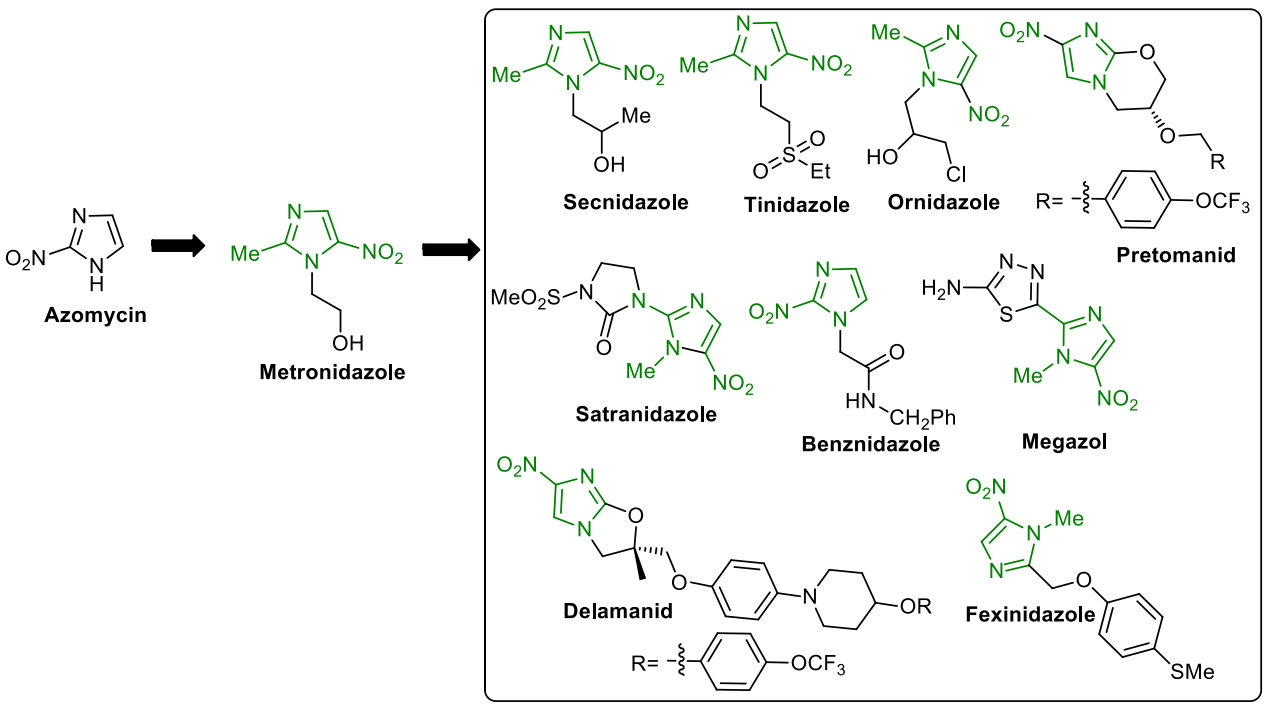

Fig. 1 Structure of nitroimidazole-based drugs for the treatment of infections caused by drug-resistant bacteria [38]

antifungal activities [31]. Metronidazole (2-methyl-5-nitroimidazole) is a synthetic derivative of azomycin with strong antibacterial and antiparasitic activities that was originally identified in cultures of *Streptomyces* species in the 1950s [36]. The azomycin (2-nitroimidazole) was the only accepted nitroimidazole relying antibiotic developed using *Actinobacteria* (*Streptomyces eurocidicus* and *Nocardia mesenterica*) and *Proteobacteria* (*Pseudomonas fluorescens*) [37]. Metronidazole (MTZ), secnidazole, tinidazole, ornidazole, satranidazole, benznidazole, pretomanid, delamanid, megazol and fexinidazole are nitroimidazoles derived from azomycin, used to treat infections caused by anaerobic Gram-positive and Gram-negative bacteria [38–40] (Fig. 1). Metronidazole acts as an antibacterial from the start because it lacks any toxicity (different from other nitroheterocycles) [41]. In general, a reactive intermediate created in the microbial reduction of the 5-nitro group of nitroimidazoles covalently binds to the microorganism's DNA and causes a lethal efficacy [41]. The objective of this study was the assessment of antibacterial and anti-biofilm effects of novel synthetized nitroimidazole compounds.

Methodology

General

All chemicals were directly applied without any additional purifications after being bought from Merck or other chemical suppliers. Certain synthetic techniques were used to create copper-doped silica cuprous sulfate (CDSCS) [42], propargyl *p*-toluenesulfonate (**3**), and 2-methyl-5-nitro-1-prop-2-ynyl-1H-imidazole (**5**) [43]. Thin-layer chromatography (TLC) was used to track reactions utilizing SILG/UV 254 silica-gel plates. The purifications was performed using column chromatography silica gel 60 (0.063–0.200 mm, 70–230 mesh; ASTM). Open capillary tubes were used to measure melting points utilizing an Electrothermal IA 9000. The elemental analyses, GC/MS, and IR spectra were obtained using the Perkine-Elmer 240-B micro-analyzer, Shimadzu GC/MS-QP 1000-EX equipment (m/z; rel.%), and Shimadzu FT-IR-8300 spectrophotometer, respectively. Using a Brüker Avance-DPX-300 spectrometer running at 300/75 MHz, the ^{1}H and ^{13}C NMR spectra were acquired. Coupling constants *J* are given in Hz, and chemical shifts are given in δ with respect to tetramethylsilane (TMS) as an internal reference [44].

Compounds 8a–8o synthesis

The ingredients including toluene, CDSCS (0.05 mol%, 0.3 g) and 10 mmol of each alkyne 5, intended cyclic amine **7** and aldehyde **6** were mixed in a flask (double-necked round bottom, 100 mL) with a condenser and heated to reflux, where TLC was used to track the reaction's development. After over 11–15 h, as shown in Table 2, TLC monitoring showed no additional improvement in the reaction progress, at which point the CDSCS was separated using a fritted glass and washed with hot EtOAc. The filtrate was then concentrated under vacuum, and the residual material was dissolved in 100 mL of $CHCl_3$ and washed with water (2 × 100 mL). After that, the organic layer was dried (Na_2SO_4) and concentrated to produce the crude product, which was then purified using appropriate elution on a short column chromatography [44].

Bacterial isolates

Bacterial standard strains included *Escherichia coli* ATCC25922, *Staphylococcus aureus* ATCC25923 and *Klebsiella pneumonia* ATCC13883. Besides, clinical isolates included 15 carbapenemase producer *E. coli* (CP-*E. coli*), two CP-*K. pneumonia*, one methicillin-susceptible *S. aureus* (MSSA) and one methicillin-resistant *S. aureus* (MRSA) isolates. The MRSA was determined using cefoxitin (30 µg) disk resistance in disk diffusion method. The ESBL production was confirmed through ceftazidime (30 µg/mL) and/or cefotaxime (30 µg/mL) resistance and synergy test between co-amoxiclav and ceftazidime/cefotaxime disks (Liofilchem, Rosetodegli Abruzzi, Italy). The carbapenemase production was determined using the combined disk (meropenem plus phenyl boronic acid and meropenem plus dipicolinic acid, Liofilchem, Rosetodegli Abruzzi, Italy) and CARBA-NP tests. The susceptibility tests were implemented according to the clinical laboratory and standards institute (CLSI) M100 version 2021 [45, 46].

Antibiotic resistance profile

The profile of antibiotic resistance among bacterial isolates was determined using the disk diffusion (Kirby Bauer) or VITEK2 compact system method according to the CLSI (clinical and laboratory standards institute) version 2023 [47]. *Pseudomonas aeruginosa* (ATCC27853), *E. coli* (ATCC25922) and *K. pneumoniae* (ATCC700603) were used as the control for verifying disks quality.

Minimum inhibitory concentration and minimum bactericidal concentration

The minimum inhibitory concentration (MIC) levels of synthetic compounds against standard and clinical bacterial isolates were determined using broth micro-dilution method in 96-well plates as per the CLSI protocol, version 2021. The bacterial suspension turbidity was equal to the half McFarland concentration. The materials range included 0.5–1024 µg/mL. The serial dilution was implemented using Mueller Hinton broth (MHB, Merck, Germany) medium (100 µL) (supplemented by 20–25 mg/L

of calcium and 10–12.5 mg/L of magnesium) plus 90 µL of compounds and 10 µL of bacterial suspension. The minimum bactericidal concentration (MBC) was determined by spot culture of 50 µL of those wells or dilutions contents without bacterial growth onto the Mueller Hinton agar (MHA) medium (Merck, Germany). Acetic acid (0.5%) and gentamicin were used as the negative and positive control of the antibacterial tests, respectively.

Biofilm formation

Biofilm formation was accomplished using microtiter tissue plate assay into 96-well plates in triplicate for each bacterial isolate. Bacterial suspension (20 µL of 10^6 CFU/mL) was added to each well containing trypticase soy broth (TSB, 180 µL; Merck, Germany) and incubated at 37 °C for 24 h. For those isolates exposed to synthetic compounds, the initial cultures were incubated for 5 h and then the wells content was replaced by 32 µg/mL and 64 µg/mL of compounds concentrations into the TSB medium and incubated for 24 h. Next, the plates were washed three times using double distilled H_2O (ddH_2O) and the wells contents were fixed using 150 µL of methanol. The wells were dried and 0.1% of crystal violet (for Gram-negative bacteria) and safranin (for Gram-positive bacteria) were added and washed after 15 min. The wells contents were solved into 96% ethanol and each turbidity was read using enzyme linked immunosorbent assay (ELISA) reader at 490 nm wavelength. The biofilm formation level for each test was calculated using following formula provided in Table 1. A strong biofilm-producer *S. aureus* isolate was used as positive control for the biofilm formation.

The in silico analyses

The in silico assessment of the binding stability of compound **8g** to the PBP2a of MRSA was implemented to verify experimental results. Firstly, the three-dimensional structure of PBP2a (PDB ID: 6H5O) was obtained from the Protein Data Bank (PDB). The AutoDockFR program was used to prepare the protein for molecular docking [48]. The ligands were processed using the OpenBabel program to add hydrogen atoms and generate a 3D structure in PDB format. A grid box size of 18.5 Å × 17.0 Å × 18.5 Å was selected to surround the catalytic site of PBP2a, which included residues E402, S403, K406, Y446, E447, S462, N464, K597, S598, and T600. The AutoDock Vina tool was utilized for conducting docking studies with the PBP2a structures and ligands in PDBQT format. Each docked complex 3D structure was analyzed using PyMOL visualization tool.

In order to estimate the stability of a complex system and study its structural flexibility, molecular dynamics (MD) simulations were conducted using GROMACS version 2022 [49, 50]. The protein molecule was parameterized using the OPLS all-atom (OPLS-AA) force field [51]. The protein–ligand complex was then placed in a simulation box and solvated with TIP3P solvent molecules [52]. The system was neutralized by adding 0.15 mol/L Na+/Cl− ions. The energy of the system was minimized using the steepest descent algorithm. The system was equilibrated using NVT and NPT ensembles with a time of 0.5 ns each, utilizing a V-rescale Berendsen thermostat and a Parrinello-Rahman barostat. The temperature of the system was gradually increased from 0 to 310 K, with the pressure set to 1 atm for the NPT ensemble. The particle-mesh Ewald (PME) and LINCS algorithms were used to calculate electrostatic interactions and restrain bond lengths in the protein, respectively [53, 54]. Periodic boundary conditions were applied during the simulation. The final coordinates of the complex system were analyzed using standard MD analyses. The final conformation of the protein–ligand complex was selected from the MD trajectory and visualized using PyMOL and LIGPLOT software. Additionally, the MMPBSA method was employed to calculate the binding free energy considering this formula: $\Delta G_{bind} = G_{complex} - (G_{protein} + G_{ligand})$ [55].

The ADMET (Adsorption, distribution, metabolism, excretion and toxicity) properties of potential candidate compound **8g** was also evaluated using pk/CSM web server.

Table 1 Biofilm formation level calculation

Biofilm formation ability	Calculation of cut-off level	OD calculated results
Strong	OD > ODc4	< 0.33296
Moderate	ODc2 ≤ OD < ODc4	0.33296 ≤ 0.16648 < OD
Weak	ODc ≤ OD < 2ODc	0.16648 ≤ 0.083324 < OD
No binding	OD ≤ ODc	0.08324 ≤ OD

OD: optical density, ODc: mean OD of control wells

Data analysis

The data was analyzed using Graph Pad Prism version 8, from which Chi-Square and analysis of variance (ANOVA) tests were applied for determination of differences at p value cut off of 0.05.

Results

Chemistry

According to the routes shown in Scheme 1, the synthesis of the designated compounds was carried out. In this synthesis pathway, 1, 2-methyl-5-nitro-1-prop-2-ynyl-1*H*-imidazole **5** was operated as an effective alkyne to prepare compounds **8a–8o**. The first step of this synthetic

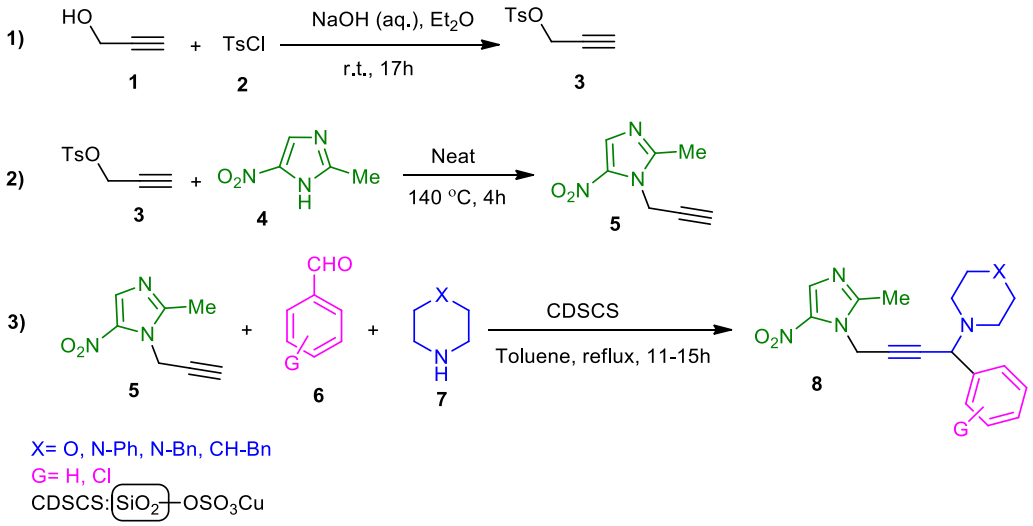

Scheme 1 Synthetic pathway for new 2-methyl-5-nitroimidazole compounds **8**

process contains the tosylation of Propargyl alcohol **1** to obtain prop-2-yn-1-yl 4-methylbenzenesulfonate **(3)** as a yellow oil [43, 56]. In the second step, 5-nitro isomer of **5** was obtained from the reaction between *N*-propargylation of 2-methyl-5-nitro-imidazole **4** with **3** under solvent-free condition [43, 57]. In other words, alkyne **5** was produced by coupling compound **4** with a propargylating factor. For this purpose, the usage of propargyl *p*-toluenesulfonate **3** would rather over propargyl bromide due to its safety, inexpensiveness and comfortable synthesis using tosylation of propargyl alcohol. Eventually, the A^3 coupling reaction between terminal alkyne **5**, aldehydes **6**, and cyclic amines **7** was carried out by copper-doped silica cuprous sulfate (CDSCS) to synthesize new derivative of 2-methyl-5-nitroimidazole propargylamines. In the following, the effect of various parameters including temperature, solvent, and catalyst amount was explored on reaction between terminal alkyne **5**, benzaldehyde, and morpholine in the attendance of CDSCS to afford 4-(4-(2-methyl- 5-nitro-1*H*-imidazole-1-yl)-1-phenylbut-2-ynyl) morpholine **(8a)** to achieve optimal condition for effective synthesis of **8a–8o** (Table 2).

According to the principle of green chemistry in doing the reaction in solvent-free conditions, the sample reaction was firstly performed in the solvent-free system. According to Table 2, the entry 1 of compound **8a** was achieved in 39% after 12 h. Thereafter, it was tried to react the sample in water and increase the reaction efficiency by increasing the temperature from room temperature to reflux. As entry 2–4 had no acceptable results, several polar and nonpolar solvents were applied. The highest yield of compound **8a** was obtained in toluene (entry 12). Entries 5–9 outlined yields from other solvents like THF, $CHCl_3$, MeCN, EtOH, and DMF giving 35–62% yields of sample compound. Consequently, toluene was used as a selective solvent for the synthesis of the defined compounds by the existing protocol. Then, the effect of temperature on the reaction progress was investigated (entries 10–12) (Table 2).

As seen in entry 12, the reaction efficiency was improved with increasing temperature, and the best outcome in toluene recovery was acquired. Considering the focus on optimizing the catalyst loading to improve and develop the reaction yield (Table 2, entries 10 and 13–17), no product was determined in the lack of CDSCS, highlighting the catalyst role in the reaction development (entry 13). Accordingly, the reaction efficiency increased at higher levels of CDSCS up to 0.05 mol% (entry 10), while further increase in the catalyst amount had no acceptable result. As a result, 0.05 mol% of CDSCS in refluxing toluene was considered as the optimal condition for the synthesis of all products. To better understand the catalytic activity and power of CDSCS, the reaction of sample A_3 coupling was carried out in the presence of some copper salts available as catalysts in reflux toluene (Table 2, entries 10 and 18–22). For **8a** compound synthesis, catalysts CuCl, CuI, Cu_2O, Cu $(OAc)_2$, and $CuSO_4.5H_2O$ had 59–73% efficiency following 15 h, while, CDSCS yielded 90% efficacy following 11 h. Moreover, the oxidation state of copper exerted no meaningful effect on the rapidity and efficiency of the reaction.

Other derivatives **8a–8o** were synthesized after achieving optimal reaction conditions (Table 3). For this purpose, alkyne **5**, various aldehydes **6** and cyclic amines 7 were subjected to the A_3 coupling reaction in the

Table 2 Influence of various reaction parameters

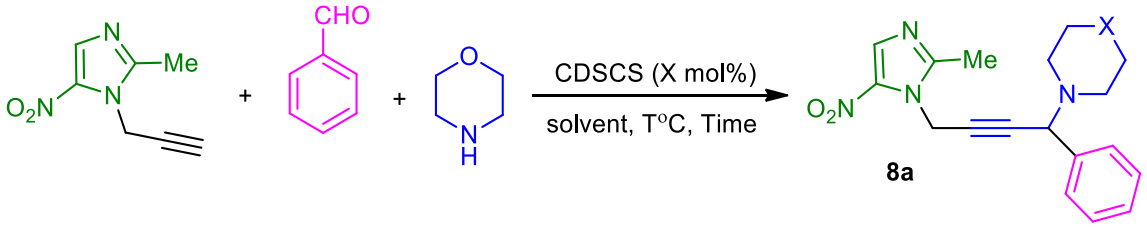

Entry	Solvent	Catalyst/mol%	T (°C)	Time (h)	Yield[a] (%)
1		CDSCS/0.05	100	12	39
2	H_2O		r.t	24	Trace
3			70	24	17
4			Reflux	14	21
5	THF			11	45
6	$CHCl_3$			15	62
7	MeCN			14	56
8	EtOH			11	35
9	DMF		110	12	51
10	Toluene		70	16	78
11	Toluene		90	14	83
12			Reflux	11	90
13		–		24	NR
14		CDSCS/0.02		24	52
15		CDSCS/0.03		18	70
16		CDSCS/0.04		14	84
17		CDSCS/0.06		11	90
18		CuCl/0.05		15	71
19		CuI/0.05		15	73
20		Cu2O/0.05		15	59
21		$Cu(OAc)_2$/0.05		15	70
22		$CuSO_4.5H_2O$/0.05		15	64

[a] Isolated yield

NR: No reaction

presence of CDSCS in reflux toluene for specified times. Four aromatic aldehydes including benzaldehyde, 4-chlorobenzaldehyde, 2,4-dichlorobenzaldehyde, and 2-chlorobenzaldehyde, and also four cyclic amines containing morpholine, 1-phenylpiperazine, 1-benzylpiperazine, and 4-benzylpiperidine were used for the synthesis of listed compounds. These aromatic aldehydes and cyclic amines were chosen due to the abundance of these parts in known drugs and active pharmaceutical compounds [58]. Considering the heterogeneous nature of CDSCS, hot filtration test was conducted to ensure the entire or adequate leaching of dissolved Cu(I) into the filtrate to continue a homogeneous reaction after solid catalyst removal [59]. The improvement of the reaction was confirmed using Gas Chromatography (GC) analysis, inferring that no additional **8a** was obtained even after 24 h. The catalytic activity was studied for **7** successive runs for the synthesis of **8a** under optimal reaction conditions to evaluate the reusability of CDSCS. For this purpose, the isolated CDSCS was washed with hot ethyl acetate and dried for 30 min at 100 °C in a vacuum oven. The recycled CDSCS was then reused in the synthesis of **8a** without addition or charge of fresh CDSCS to the reaction mixture. According to Inductively Coupled Plasma (ICP) analysis, 0.01% Cu was eluted from CDSCS after seven repetitions, highlighting thermal and chemical stability of the catalyst under optimal reaction conditions.

In Scheme 2, a possible mechanism has been inferred for the synthesis of compounds **8a** by the A_3 coupling

Table 3 Isolated structures and yields of synthesized compounds **8a**–**8o**

Structure	Yield	Time
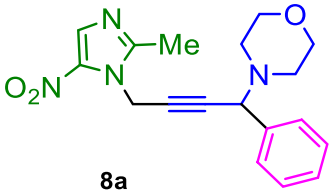 **8a**	90%	11h
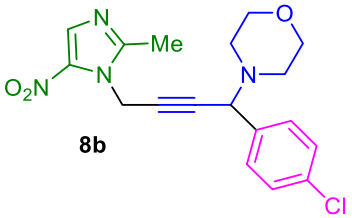 **8b**	89%	11h
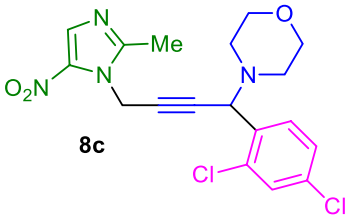 **8c**	86%	13h
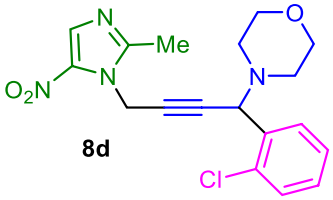 **8d**	82%	15h
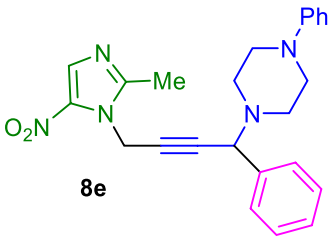 **8e**	88%	11h
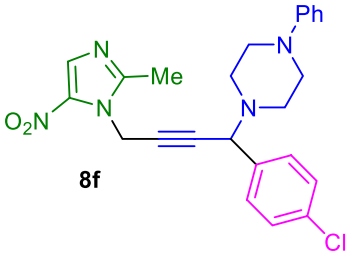 **8f**	85%	11h

Table 3 (continued)

Structure	Yield	Time
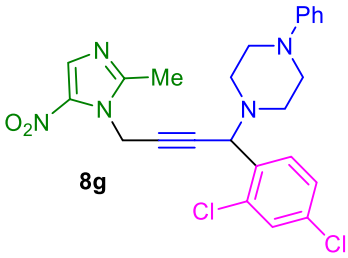 **8g**	83%	12h
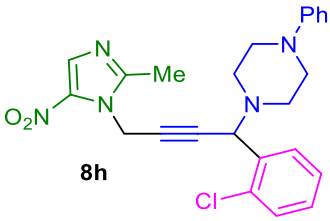 **8h**	81%	14h
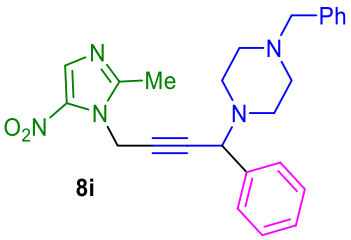 **8i**	93%	11h
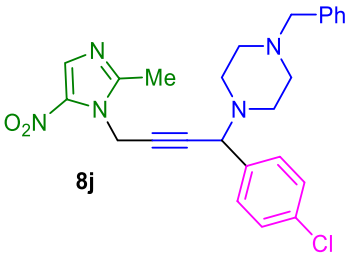 **8j**	91%	12h
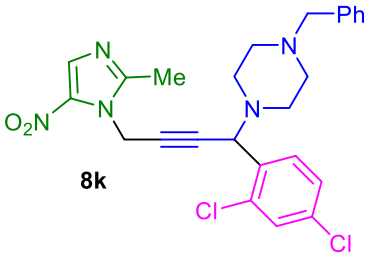 **8k**	89%	12h

reaction of sample substrates in the presence of CDSCS [60]. Initially, the C-H activation of alkyne 7 with the nanocatalyst forms the π-alkyne complex I, which is converted to the copper acetylide adduct III. At the same time, the condensation of benzaldehyde with morpholine leads to the in situ production of iminium ion II. Finally,

Table 3 (continued)

Structure	Yield	Time
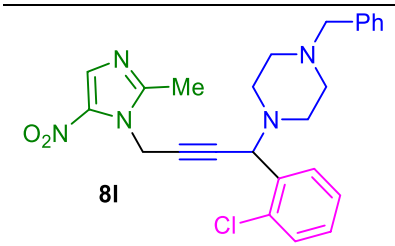 **8l**	83%	15h
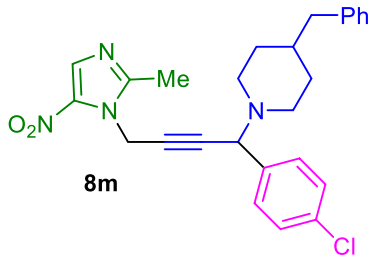 **8m**	89%	11h
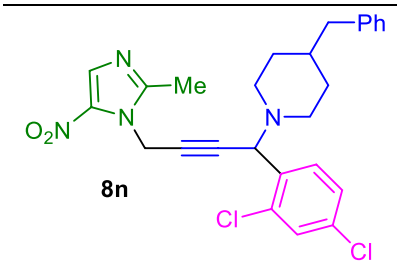 **8n**	84%	12h
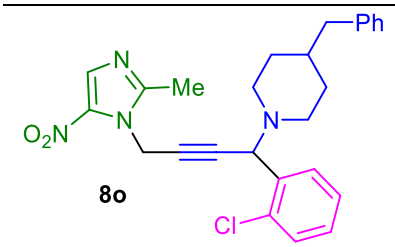 **8o**	81%	14h

compounds **8a** is generated by nucleophilic addition of adduct III to iminium ion II, and regenerated the catalyst for subsequent catalytic run. After the compounds synthesis, they were dissolved into 0.5% acetic acid.

NMR Data of synthesized compounds

The NMR data of synthesized compounds has been included below and in the supplementary data file as previously determined [44].

4-(4-(2-methyl-5-nitro-1H-imidazole-1-yl)-1-phenylbut-2-ynyl) morpholine (8a)

Column Chromatography (SiO_2) eluted with n-hexane:EtOAc (1:2) afforded pure product as white solid (3.06 g, 90%); m. p, 153e155 °C. IR (KBr): 3100, 2954, 2169, 1671, 1560, 1485, 1352 cm^{-1}.^{1}H NMR ($CDCl_3$, 300 MHz) δ_{ppm} = 2.49–2.51 (complex, 7H, CH_3, 2 NCH_2), 3.68–3.71 (m, 4H, $2OCH_2$), 4.59 (s, 1H, NCH), 4.84 (s, 2H, $NCH_2C{\equiv}C$), 7.26–7.38 (m, 3H, aryl), 7.45–7.47 (m, 2H, aryl), 7.89 (s, 1H, C(5)-H, imidazole). ^{13}C NMR ($CDCl_3$, 75 MHz) δ_{ppm} = 14.30, 26.61, 49.72, 60.23, 66.55, 81.86, 84.56, 127.21, 128.42, 128.95, 131.74, 138.03, 139.85, 151.85. MS (EI): m/z (%) = 340 (21.5) [M^+]. Anal. Calc. for $C_{18}H_{20}N_4O_3$: C, 63.52; H, 5.92; N, 16.46; found: C, 63.70; H, 6.08; N, 16.61.

4-(1-(4-chlorophenyl)-4-(2-methyl-5-nitro-1H-imidazole-1-yl) but-2-ynyl) morpholine (8b)

Column Chromatography (SiO_2) eluted with n-hexane:EtOAc (1) afforded pure product as white solid (3.33 g, 89%); m. p,171–173 °C. IR (KBr): 3068, 2950, 2180, 1678, 1552, 1481, 1350, 1125 cm^{-1}.^{1}H NMR ($CDCl_3$, 300 MHz) δ_{ppm} = 2.47–2.59 (complex, 7H, CH_3, 2 NCH_2), 3.68–3.71 (m, 4H, $2OCH_2$), 4.58 (s, 1H, NCH), 4.85 (s, 2H, $NCH_2C{\equiv}C$), 7.24–7.28 (m, 1H, aryl), 7.31–7.34 (m, 1H, aryl), 7.40–7.43 (m, 2H, aryl), 7.89 (s, 1H, C(5)-H, imidazole). ^{13}C NMR ($CDCl_3$, 75 MHz) δ_{ppm} = 13.75, 26.72, 49.89, 58.83, 66.22, 82.28, 85.07, 128.60, 130.48, 131.69, 132.94, 138.21, 151.80. MS (EI): m/z (%) = 374 (23.8) [M^+]. Anal. Calc. for $C_{18}H_{19}ClN_4O_3$: C, 57.68; H, 5.11; N, 14.95; found: C, 57.95; H, 5.26; N, 15.09.

4-(1-(2,4-dichlorophenyl)-4-(2-methyl-5-nitro-1H-imidazole-1-yl)but-2-ynyl)morpholine (8c)

Column Chromatography (SiO_2) eluted with *n*-hexane:EtOAc (2:5) afforded pure product as white solid (3.51 g, 86%); m. p, 143–145 °C. IR (KBr): 3070, 2973, 2148, 1676, 1556, 1459, 1354, 1128 cm^{-1}.^{1}H NMR ($CDCl_3$, 300 MHz) δ_{ppm} = 2.48–2.54 (complex, 7H, CH_3, $2NCH_2$), 3.64–3.68 (m, 4H, $2OCH_2$), 4.82 (s, 2H, $NCH_2C{\equiv}C$), 4.87 (s, 1H, NCH), 7.24–7.27 (m, 1H, aryl), 7.42–7.47 (m, 2H, aryl), 7.83 (s, 1H, C(5)-H, imidazole). ^{13}C NMR ($CDCl_3$, 75 MHz) δ_{ppm} = 13.70, 26.64, 49.79, 51.94, 66.15, 81.86, 84.95, 126.59, 129.97, 131.53, 131.83, 134.29, 134.91, 135.85, 138.30, 151.86. MS (EI): m/z (%) = 408 (27.9) [M^+]. Anal. Calc. for $C_{18}H_{18}Cl_2N_4O_3$: C, 52.82; H, 4.43; N, 13.69; found: C, 52.98; H, 4.57; N, 13.83.

4-(1-(2-chlorophenyl)-4-(2-methyl-5-nitro-1H-imidazole-1-yl) but-2-ynyl) morpholine (8d)

Column Chromatography (SiO_2) eluted with *n*-hexane: EtOAc (1:2) afforded pure product as creamy solid (3.07 g, 82%); m. p, 169–171 °C. IR (KBr): 3037, 2965, 2193, 1690, 1568, 1463, 1357, 1140 cm^{-1}.^{1}H NMR ($CDCl_3$, 300 MHz) δ_{ppm} = 2.45 (s, 3H, CH_3), 2.51 (br s, 4H, $2NCH_2$), 3.57–3.69 (m, 4H, $2OCH_2$), 4.82 (s, 2H,

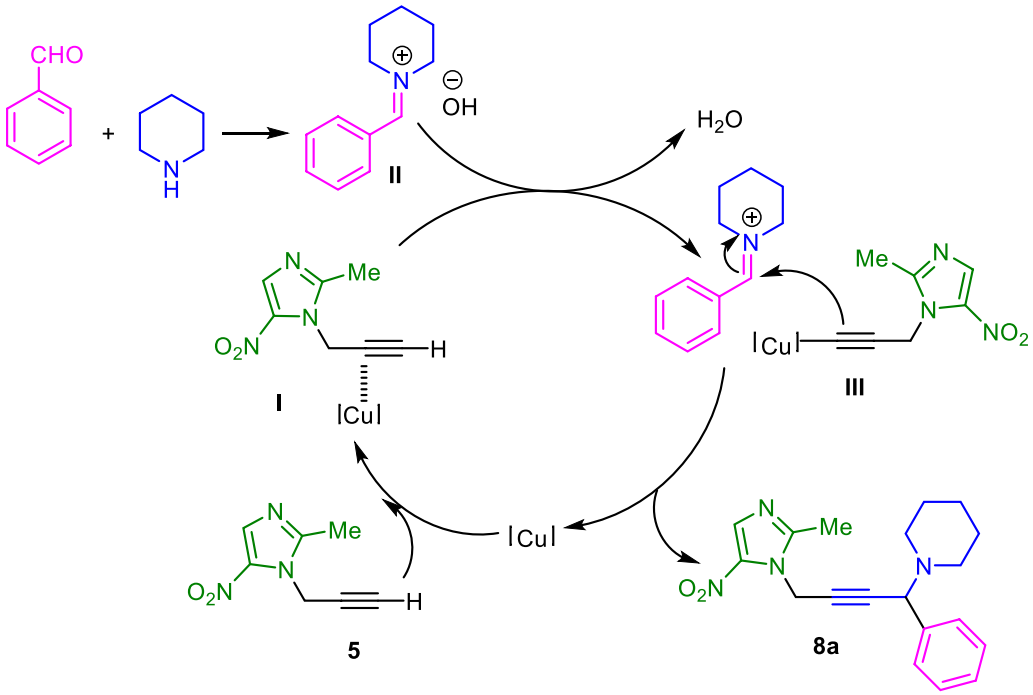

Scheme 2 Synthesis mechanism of **8a** in the presence of CDSCS

$NCH_2C{\equiv}C$), 4.91 (s, 1H, NCH), 7.11–7.25 (m, 2H, aryl), 7.34–7.38 (m, 1H, aryl), 7.48–7.51 (m, 1H, aryl), 7.85 (s, 1H, C(5)-H, imidazole). ^{13}C NMR ($CDCl_3$, 75 MHz) δ_{ppm} = 14.20, 26.18, 49.78, 51.74, 66.40, 81.70, 84.70, 126.56, 128.62, 128.91, 129.91, 131.90, 134.25, 136.88, 138.22, 151.86. MS (EI): m/z (%) = 374 (19.6) [M^+]. Anal. Calc. for $C_{18}H_{19}ClN_4O_3$: C, 57.68; H, 5.11; N, 14.95; found: C, 57.45; H, 5.26; N, 14.80.

1-(4-(2-methyl-5-nitro-1H-imidazole-1-yl)-1-phenylbut-2-ynyl)-4-phenylpiperazine (8e)

Column Chromatography (SiO_2) eluted with *n*-hexane: EtOAc (1:2) afforded pure product as bright brown solid (3.65 g, 88%); m. p, 181–183 °C. IR (KBr): 3055, 2947, 2186, 1680, 1554, 1479, 1350 cm^{-1}.^{1}H NMR ($CDCl_3$, 300 MHz) δ_{ppm} = 2.48 (s, 3H, CH_3), 2.67 (br s, 4H, $2NCH_2$), 3.18 (br s, 4H, $2PhNCH_2$), 4.67 (s, 1H, NCH), 4.78 (s, 2H, $NCH_2C{\equiv}C$), 6.75–6.91 (m, 3H, aryl), 7.16–7.39 (m, 5H, aryl), 7.48 (d, J = 7.5 Hz, 2H, aryl), 7.86 (s, 1H, C(5)-H, imidazole). ^{13}C NMR ($CDCl_3$, 75 MHz) δ_{ppm} = 13.93, 26.70, 48.60, 49.57, 60.71, 82.00, 85.59, 114.37, 118.29, 127.47, 128.45, 128.76, 129.75, 131.71, 138.25, 139.87, 149.71, 151.66. MS (EI): m/z (%) = 415 (21.6) [M^+]. Anal. Calc. for $C_{24}H_{25}N_5O_2$: C, 69.38; H, 6.06; N, 16.86; found: C, 69.53; H, 6.19; N, 17.02.

1-(1-(4-chlorophenyl)-4-(2-methyl-5-nitro-1H-imidazole-1-yl)but-2-ynyl)-4-phenylpiperazine (8f)

Column Chromatography (SiO_2) eluted with *n*-hexane:EtOAc (1:2) afforded pure product as bright brown solid (3.82 g, 85%); m. p, 201–203 °C. IR (KBr): 3027, 2930, 2129, 1677, 1553, 1426, 1347, 1160 cm^{-1}.^{1}H NMR ($CDCl_3$, 300 MHz) δ_{ppm} = 2.49 (s, 3H, CH_3), 2.55–2.70 (m, 4H, $2NCH_2$), 3.13–3.22 (m, 4H, $2PhNCH_2$), 4.68 (s, 1H, NCH), 4.84 (s, 2H, $NCH_2C{\equiv}C$), 6.80–6.91 (m, 3H, aryl), 7.20–7.28 (m, 4H, aryl), 7.32–7.46 (m, 2H, aryl), 7.85 (s, 1H, C(5)-H, imidazole). ^{13}C NMR ($CDCl_3$, 75 MHz) δ_{ppm} = 13.59, 26.18, 48.39, 49.95, 60.61, 82.05, 85.89, 114.96, 119.18, 128.40, 128.73, 129.50, 131.81, 132.57, 138.32, 139.81, 149.39, 151.69. MS (EI): m/z (%) = 449 (18.7) [M^+]. Anal. Calc. for $C_{24}H_{24}ClN_5O_2$: C, 64.07; H, 5.38; N, 15.57; found: C, 64.29; H, 5.56; N, 15.74.

1-(1-(2,4-dichlorophenyl)-4-(2-methyl-5-nitro-1H-imidazole-1-yl)but-2-ynyl)-4-phenylpiperazine (8g)

Column Chromatography (SiO_2) eluted with *n*-hexane: EtOAc (1:2) afforded pure product as bright brown solid (4.02 g, 83%); m. p, 157–159 °C. IR (KBr): 3084, 2938, 2170, 1688, 1558, 1448, 1353, 1161 cm^{-1}.^{1}H NMR ($CDCl_3$, 300 MHz) δ_{ppm} = 2.46 (s, 3H, CH_3), 2.69–2.70 (m, 4H, $2NCH_2$), 3.10 3.20 (m, 4H, $2PhNCH_2$), 4.82 (s, 2H, $NCH_2C{\equiv}C$), 4.96 (s, 1H, NCH), 6.79–6.90 (m, 3H, aryl), 7.22–7.29 (m, 3H, aryl), 7.39 (s, 1H, aryl), 7.48 (d,

J = 8.1 Hz, 1H, aryl), 7.82 (s, 1H, C(5)-H, imidazole). ^{13}C NMR ($CDCl_3$, 75 MHz) δ_{ppm} = 13.32, 27.02, 48.76, 49.96, 52.37, 83.77, 87.81, 114.37, 118.79, 126.83, 129.71, 130.02, 131.30, 131.70, 134.09, 134.91, 135.69, 138.10, 149.80, 151.78. MS (EI): m/z (%) = 483 (22.6) [M^+]. Anal. Calc. for $C_{24}H_{23}Cl_2N_5O_2$: C, 59.51; H, 4.79; N, 14.46; found: C, 59.38; H, 4.60; N, 14.32.

1-(1-(2-chlorophenyl)-4-(2-methyl-5-nitro-1H-imidazole-1-yl) but-2-ynyl)-4-phenylpiperazine (8h)

Column Chromatography (SiO_2) eluted with *n*-hexane: EtOAc (1:2) afforded pure product as pale yellow solid (3.64 g, 81%); m. p, 197–199 °C. IR (KBr): 3100, 2951, 2192, 1682, 1559, 1441, 1350, 1134 cm^{-1}.^{1}H NMR ($CDCl_3$, 300 MHz) δ_{ppm} = 2.44 (s, 3H, CH_3), 2.70–2.71 (m, 4H, $2NCH_2$), 3.09–3.20 (m, 4H, $2PhNCH_2$), 4.79 (s, 2H, $NCH_2C{\equiv}C$), 5.02 (s, 1H, NCH), 6.74–6.90 (m, 3H, aryl), 7.21–7.29 (m, 4H, aryl), 7.39–7.41 (m, 1H, aryl), 7.54–7.55 (m, 1H, aryl), 7.83 (s, 1H, C(5)-H, imidazole). ^{13}C NMR ($CDCl_3$, 75 MHz) δ_{ppm} = 13.70, 26.93, 48.91, 49.85, 52.06, 83.19, 86.96, 114.32, 118.41, 126.61, 128.48, 128.80, 129.74, 130.37, 131.91, 134.44, 136.66, 138.22, 149.57, 151.76. MS (EI): m/z (%) = 449 (26.1) [M^+]. Anal. Calc. for $C_{24}H_{24}ClN_5O_2$: C, 64.07; H, 5.38; N, 15.57; found: C, 64.29; H, 5.61; N, 15.72.

1-Benzyl-4-(4-(2-methyl-5-nitro-1H-imidazole-1-yl)-1-phenylbut-2-ynyl) piperazine (8i)

Column Chromatography (SiO_2) eluted with *n*-hexane: EtOAc (1:2) afforded pure product as creamy solid (3.99 g, 93%); m. p, 139–141 °C. IR (KBr): 3080, 2951, 2146, 1659, 1559, 1465, 1357 cm^{-1}.^{1}H NMR ($CDCl_3$, 300 MHz) δ_{ppm} = 2.33–2.52 (complex, 11H, CH_3, $2NCH_2CH_2N$), 3.49 (s, 2H, NCH_2Ph), 4.61 (s, 1H, NCH), 4.81 (s, 2H, $NCH_2C{\equiv}C$), 7.16–7.45 (complex, 10H, aryl), 7.86 (s, 1H, C(5)-H, imidazole). ^{13}C NMR ($CDCl_3$, 75 MHz) δ_{ppm} = 12.75, 25.65, 49.23, 51.42, 53.97, 60.85, 84.13, 88.88, 127.21, 128.48, 128.80, 131.91, 135.70, 138.22, 139.79, 151.76. MS (EI): m/z (%) = 429 (17.6) [M^+]. Anal. Calc. for $C_{25}H_{27}N_5O_2$: C, 69.91; H, 6.34; N, 16.31; found: C, 69.76; H, 6.20; N, 16.14.

1-Benzyl-4-(1-(4-chlorophenyl)-4-(2-methyl-5-nitro-1H-imidazole-1-yl)but-2-ynyl)piperazine (8j)

Column Chromatography (SiO_2) eluted with *n*-hexane: EtOAc (1:2) afforded pure product as brown solid (4.22 g, 91%); m. p,171–173 °C. IR (KBr): 3041, 2930, 2152, 1679, 1553, 1470, 1361, 1169 cm^{-1}.^{1}H NMR ($CDCl_3$, 300 MHz) δ_{ppm} = 2.33–2.48 (complex, 11H, CH_3, $2NCH_2CH_2N$), 3.44 (s, 2H, NCH_2Ph), 4.62 (s, 1H, NCH), 4.82 (s, 2H, $NCH_2C{\equiv}C$), 7.12–7.40 (complex, 9H, aryl), 7.85 (s, 1H, C(5)-H, imidazole). ^{13}C NMR ($CDCl_3$, 75 MHz) δ_{ppm} = 13.07, 27.22, 49.23, 51.42, 53.32, 61.17, 83.51, 87.60, 127.21, 128.16, 128.48, 128.80, 130.37, 131.91, 132.87, 135.70, 138.22, 151.76. MS (EI): m/z (%) = 463 (24.7) [M^+]. Anal. Calc. for $C_{25}H_{26}ClN_5O_2$: C, 64.72; H, 5.65; N, 15.09; found: C, 64.90; H, 5.81; N, 15.26.

1-Benzyl-4-(1-(2,4-dichlorophenyl)-4-(2-methyl-5-nitro-1Himidazole-1-yl)but-2-ynyl)piperazine (8k)

Column Chromatography (SiO_2) eluted with *n*-hexane: EtOAc (1:2) afforded pure product as creamy solid (4.43 g, 89%); m. p, 113–115 °C. IR (KBr): 3079, 2938, 2149, 1654, 1558, 1460, 1353, 1129 cm^{-1}.^{1}H NMR ($CDCl_3$, 300 MHz) δ_{ppm} = 2.34–2.54 (complex, 11H, CH_3, $2NCH_2CH_2N$), 3.48 (s, 2H, NCH_2Ph), 4.79 (s, 2H, $NCH_2C{\equiv}C$), 4.89 (s, 1H, NCH), 7.15–7.36 (m, 6H, aryl), 7.40–7.49 (m, 2H, aryl) 7.83 (s, 1H, C(5)-H, imidazole). ^{13}C NMR ($CDCl_3$, 75 MHz) δ_{ppm} = 12.75, 26.28, 47.49, 49.85, 52.06, 60.25, 83.19, 85.72, 126.61, 127.21, 128.48, 128.80, 130.04, 131.60, 131.91, 134.12, 134.78, 135.70, 138.22, 151.76. MS (EI): m/z (%) = 497 (16.9) [M^+]. Anal. Calc. for $C_{25}H_{25}Cl_2N_5O_2$: C, 60.25; H, 5.06; N, 14.05; found: C, 60.39; H, 5.22; N, 14.19.

1-Benzyl-4-(1-(2-chlorophenyl)-4-(2-methyl-5-nitro-1Himidazole-1-yl)but-2-ynyl)piperazine (8l)

Column Chromatography (SiO_2) eluted with *n*-hexane: EtOAc (1:1) afforded pure product as creamy solid (3.85 g, 83%); m. p, 137–139 °C. IR (KBr): 3060, 2966, 2119, 1674, 1559, 1465, 1349, 1162 cm^{-1}.^{1}H NMR ($CDCl_3$, 300 MHz) δ_{ppm} = 2.39–2.68 (complex, 11H, CH_3, $2NCH_2CH_2N$), 3.48 (s, 2H, NCH_2Ph), 4.78 (s, 2H, $NCH_2C{\equiv}C$), 4.97 (s, 1H, NCH), 7.11–7.29 (complex, 7H, aryl), 7.36–7.40 (m, 1H, aryl), 7.48–7.50 (m, 1H, aryl), 7.85 (s, 1H, C(5)-H, imidazole). ^{13}C NMR ($CDCl_3$, 75 MHz) δ_{ppm} = 13.34, 26.88, 48.44, 49.06, 51.83, 60.44, 83.20, 86.58, 126.61, 127.24, 128.16, 128.46, 128.78, 129.03, 130.30, 131.85, 134.32, 135.55, 136.77, 138.33, 151.84. MS (EI): m/z (%) = 463 (19.5) [M^+]. Anal. Calc. for $C_{25}H_{26}ClN_5O_2$: C, 64.72; H, 5.65; N, 15.09; found: C, 64.53; H, 5.49; N, 14.85.

4-Benzyl-1-(1-(4-chlorophenyl)-4-(2-methyl-5-nitro-1Himidazole- 1-yl) but-2-yn-1-yl) piperidine (8m) Column Chromatography (SiO_2) eluted with *n*-hexane:EtOAc (5:2) afforded pure product as creamy solid (4.12 g, 89%); m. p, 124–126 °C. IR (KBr): 3100, 2959, 2163, 1659, 1563, 1480, 1355, 1165 cm^{-1}.^{1}H NMR ($CDCl_3$, 300 MHz) δ_{ppm} = 1.36–1.69 (complex, 5H, CH_2CHCH_2), 1.95–1.97 (m, 1H, $PhCH_AH_B$), 2.26–2.27 (m, 1H, $PhCH_AH_B$), 2.39–2.57 (complex, 5H, NCH_2, CH_3), 2.82–2.86 (m, 2H, NCH_2), 4.59 (s, 1H, NCH), 4.81 (s, 2H, $NCH_2C{\equiv}C$), 7.02–7.41 (m, 9H, aryl), 7.86 (s, 1H, C(5)-H, imidazole). ^{13}C NMR ($CDCl_3$, 75 MHz) δ_{ppm} = 12.91, 24.76, 26.69, 29.58, 40.11, 48.77, 55.84, 84.01, 87.87,

126.02, 128.21, 128.86, 130.48, 131.73, 132.70, 138.15, 138.80, 151.95. MS (EI): m/z (%) = 462 (25.3) [M^+]. Anal. Calc. for $C_{26}H_{27}ClN_4O_2$: C, 67.45; H, 5.88; N, 12.10; found: C, 67.64; H, 6.07; N, 12.32.

4-Benzyl-1-(1-(2,4-dichlorophenyl)-4-(2-methyl-5-nitro-1Himidazole-1-yl) but-2-ynyl) piperidine (8n) Column Chromatography(SiO_2) eluted with *n*-hexane:EtOAc (2:1) afforded pure product as creamy solid (4.17 g, 84%); m. p, 114–116 °C. IR (KBr): 3024, 2926, 2173, 1673, 1537, 1423, 1351, 1134 cm^{-1}.^{1}H NMR ($CDCl_3$, 300 MHz) δ_{ppm} = 1.06–1.29 (m, 2H, CH_2CH), 1.56–1.64 (complex, 3H, CH_2CH), 2.00–2.07 (m, 1H, $PhCH_AH_B$), 2.15–2.23 (m, 1H, $PhCH_AH_B$), 2.40–2.50 (complex, 5H, NCH_2, CH_3), 2.73–2.84 (m, 2H, NCH_2), 4.77 (s, 2H, $NCH_2C{\equiv}C$), 4.85 (s, 1H, NCH), 7.09–7.28 (m, 7H, aryl), 7.39–7.45 (m, 1H, aryl), 7.82 (s, 1H, C(5)-H, imidazole). ^{13}C NMR ($CDCl_3$, 75 MHz) δ_{ppm} = 12.91, 24.76, 26.69, 29.24, 40.11, 48.77, 50.70, 83.37, 85.94, 126.02, 126.96, 128.21, 128.86, 130.17, 131.73, 132.06, 134.32, 134.97, 135.59, 138.15, 138.80, 151.95. MS (EI): m/z (%) = 496 (27.4) [M^+]. Anal. Calc. for $C_{26}H_{26}Cl_2N_4O_2$: C, 62.78; H, 5.27; N, 11.26; found: C, 62.60; H, 5.07; N, 11.10.

4-Benzyl-1-(1-(2-chlorophenyl)-4-(2-methyl-5-nitro-1Himidazole-1-yl)but-2-yn-1-yl)piperidine (8o) Column Chromatography(SiO_2) eluted with *n*-hexane:EtOAc (5:2) afforded pure product as white solid (3.75 g, 81%); m. p, 160–162 °C. IR (KBr): 3100, 2937, 2172, 1683, 1552, 1450, 1327, 1126 cm^{-1}.^{1}H NMR ($CDCl_3$, 300 MHz) δ_{ppm} = 1.46–1.63 (complex, 5H, CH_2CHCH_2), 2.05–2.08 (m, 1H, $PhCH_AH_B$), 2.20–2.23 (m, 1H, $PhCH_AH_B$), 2.39–2.50 (complex, 5H, NCH_2, CH_3), 2.83–2.87 (m, 2H, NCH_2), 4.77 (s, 2H, $NCH_2C{\equiv}C$), 4.93 (s, 1H, NCH), 7.09–7.28 (m, 7H, aryl), 7.39 (d, J = 8.1 Hz, 1H, aryl), 7.50 (d, J = 8.1 Hz, 1H, aryl), 7.83 (s, 1H, C(5)-H, imidazole). ^{13}C NMR ($CDCl_3$, 75 MHz) δ_{ppm} = 13.27, 24.62, 26.89, 29.48, 40.50, 48.59, 51.50, 82.00, 86.21, 126.09, 126.73, 128.03, 128.46, 128.68, 130.31, 131.79, 134.20, 136.79, 138.09, 138.74, 151.70. MS (EI): m/z (%) = 463 (22.6) [M^+]. Anal. Calc. for $C_{25}H_{26}ClN_5O_2$: C, 64.72; H, 5.65; N, 15.09; found: C, 64.95; H, 5.83; N, 15.30.

Susceptibility profile of isolates

According to the supplementary Tables S1, S2 and S3, among CP-*E. coli* and CP-*K. pneumonia,* all of them were resistant to amoxicillin/clavulanic acid, ampicillin/sulbactam, ticarcillin/clavulanic acid, cefazolin, ertapenem, cefuroxime and cefotaxime. However, lowest resistance was against nitrofurantoin (5/15 or 33% for CP-*E. coli* and 1/2 or 50% for CP-*K. pneumonia*), tigecycline (1/15 or 6.6% for CP-*E. coli* and 0% for CP-*K. pneumonia*) and polymyxin B (1/15 6.6% for CP-*E. coli* and 0% for CP-*K. pneumonia*). Additionally, 50% (1/2) of CP-*K. pneumonia* isolates were susceptible to amikacin. MSSA and MRSA isolates were resistant to penicillin, erythromycin and clindamycin, while both of them were susceptible to vancomycin, minocycle and linezolid. MSSA was also susceptible to rifampin, gentamicin, minocycline, sulfamethoxazole-trimethoprim (TMP-SMX) and levofloxacin. MRSA also exhibited resistance to TMP-SMX, levofloxacin and gentamicin and intermediate resistance to rifampin.

The MIC and MBC determination

The MIC and MBC levels of synthetic compounds against standard and clinical bacterial isolates has been depicted in Tables 4 and 5 and Figs. 2, 3, 4, 5, 6. Accordingly, the lowest MIC/MBC levels corresponded to compound **8g** against standard *S. aureus* (1/2 µg/mL) and *K. pneumonia* (8/32 µg/mL) standard and clinical strains. Additionally, there was a significant difference between clinical and standard strains of *E. coli* regarding MIC and MBC levels of compounds **8h**, **8k**, **8l**, **8n** and **8o** which exhibited lower levels against standard strain. Considering *K. pneumonia*, there was also a significant difference between clinical and standard strains for compounds **8b**–**8e**, **8j**, **8k** and **8o**. Compounds **8a**–**8e** exerted higher antibacterial effects against clinical *K. pneumonia* and *S. aureus* compared to *E. coli* isolates. Compound **8i** inferred low MIC and MBC (16 and 32 µg/mL, respectively) against *E. coli*. Interestingly, compounds **8i**–**8o** conferred significant higher antibacterial effects against Gram-negative strains. Furthermore, there was no significant difference in MIC or MBC values between *S. aureus* standard strain and each of clinical MSSA/MRSA. The MIC of metronidazole against CP-*E. coli,* CP-*K. pneumonia,* MSSA and MRSA respectively ranged 32–64 µg/mL, 32–128 µg/mL, 16 µg/mL and 64 µg/mL. Additionally, metronidazole MBC levels against CP-*E. coli,* CP-*K. pneumonia,* MSSA and MRSA respectively ranged 32–128 µg/mL, 64–256 µg/mL, 32 µg/mL and 128 µg/mL. Acetic acid (0.5%) has no growth-inhibitory effect against bacterial isolates.

Also, Fig. 6 depicts the significant lower MIC levels of synthetic compounds than metronidazole against bacterial isolates in this study.

Structure–activity relationship

From a structure–activity relationship (SAR) perspective, the synthesized nitroimidazole compounds can be categorized into three distinct groups based on their amine moieties. Additionally, considering the apparent biological activity of chloroaryl moieties in many established drugs, particularly concerning their antibacterial profiles, aryl residues were preferentially designed to include a chlorine group. In this context, the first group

Table 4 The MIC and MBC concentrations of synthetic compounds against *E. coli* and *K. pneumonia* standard and clinical isolates

Compound/Bacteria	*E. coli* S; MIC/MBC (μg/mL)	*E. coli* C; MIC/MBC (μg/mL)	*K. pneumonia* S; MIC/MBC (μg/mL)	*K. pneumonia* C; MIC/MBC (μg/mL)	*p value*
8a	32/128	32/128	16/64	16/64	> 0.05
8b	32/128	64/128	64/128	16/64*	< 0.001
8c	32/128	32/128	32/128	16/64*	< 0.001
8d	32/128	32/128	32/128	16/64*	< 0.001
8e	32/64	32/128	32/128	16/64*	< 0.001
8f	32/128	128/256	32/64	16/64	< 0.001
8g	32/128	32/128	8/32	8/32	0.998
8h	16/64	64/256*	16/64	16/64	< 0.001
8i	16/32	16/32	16/64	32/64	> 0.05
8j	16/64	32/64	32/128	16/64*	< 0.001
8k	16/64	32/128*	32/64	64/128*	< 0.001
8l	16/64	32/128*	16/64	16/64	< 0.001
8m	16/64	16/64	16/64	16/64	> 0.05
8n	16/64	32/128*	32/128	16/64*	< 0.001
8o	16/64	32/128*	32/64	16/64	< 0.001
Metronidazole	8/16	32/64	8/16	64/128	< 0.001

E. coli S: *Escherichia coli* standard strain, *E. coli* C: carbapenemase-producing *E. coli*, *K. pneumonia* S: *Klebsiella pneumonia* standard strain, *K. pneumonia* C: carbapenemase-producing *K. pneumonia*, MIC: minimum inhibitory concentration, MBC: minimum bactericidal concentration, *indicating significant difference

Table 5 The MIC and MBC concentrations of synthetic compounds against *S. aureus* standard and clinical isolates

Compound/Bacteria	*S. aureus* S; MIC/MBC (μg/mL)	MSSA; MIC/MBC (μg/mL)	MRSA; MIC/MBC (μg/mL)	*p* value
8a	32/128	32/128	32/128	> 0.05
8b	16/64	16/64	16/64	> 0.05
8c	16/64	16/64	16/64	> 0.05
8d	16/64	16/64	16/64	> 0.05
8e	16/64	16/64	16/64	> 0.05
8f	32/128	32/128	32/128	> 0.05
8g	1/2	1/2	1/2	> 0.05
8h	32/128	32/128	32/128	> 0.05
8i	64/256	64/256	64/256	> 0.05
8j	64/256	64/256	64/256	> 0.05
8k	64/256	64/256	64/256	> 0.05
8l	64/256	64/256	64/256	> 0.05
8m	64/256	64/256	64/256	> 0.05
8n	64/256	64/256	64/256	> 0.05
8o	64/256	64/256	64/256	> 0.05
Metronidazole	4/8	16/32	64/128	< 0.0001

features morpholine residues (**8a**–**8d**), with all members demonstrating superior antibacterial effects compared to metronidazole, particularly against *K. pneumonia* (16/64 μg/mL). The second group consists of piperazine residues (**8e**–**8h**), which exhibited potent antibacterial activity against all tested bacteria; notably, compound **8g** showed remarkable inhibitory effects against both standard and clinical strains of *S. aureus* (1/2 μg/mL) and *K. pneumonia* (8/32 μg/mL). The significant biological activity of this second family may be attributed to the presence of the piperazine moiety, known for its antibacterial properties. The third group contains compounds with a 4-phenylpiperazine moiety (**8i**–**8o**), which, similar to the second group, exhibited strong antibacterial activity against all tested bacteria. Among these, compounds **8j** and **8m** demonstrated enhanced activity against *E. coli*,

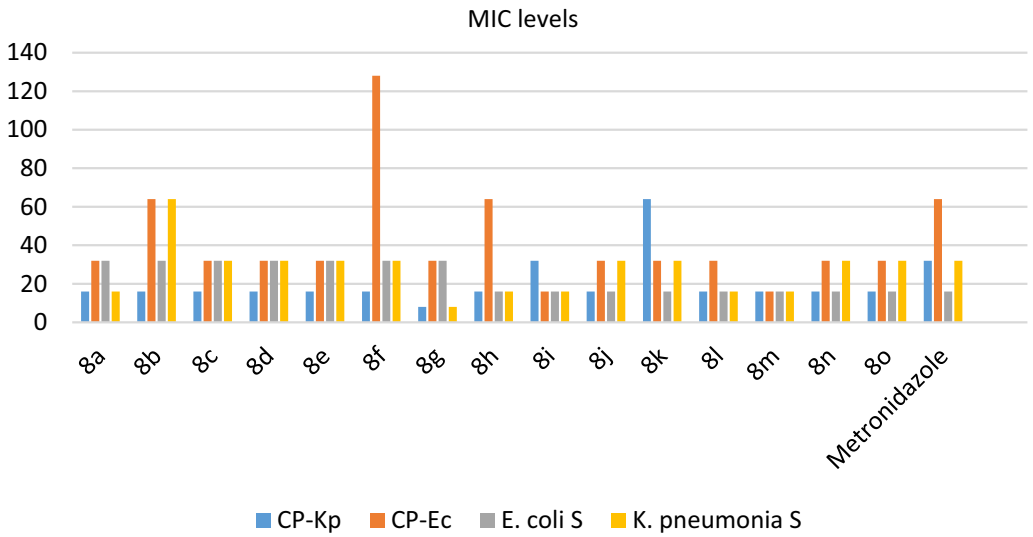

Fig. 2 MIC levels of nitroimidazole compounds against gram-negative bacteria in this study; *E. coli* S: *Escherichia coli* ATCC25922, *K. pneumonia* S: *Klebsiella pneumonia* ATCC13883. CP-*E. coli*: carbapenemase producer *E. coli*, CP-*K. pneumonia*: carbapenemase producer *K. pneumonia*. In comparison to metronidazole, against CP-*E. coli*, compounds **8i** and **8m** had significantly higher antibacterial effects ($p < 0.001$) and against CP-*K. pneumonia*, compounds **8a**–**8j** and **8l**–**8o** had significantly higher ($p < 0.0001$) antibacterial effects

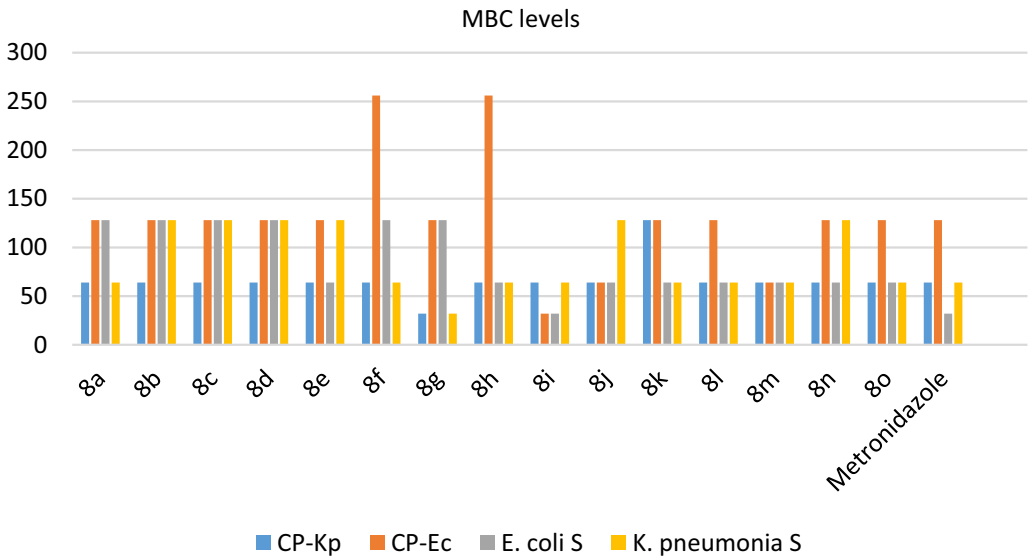

Fig. 3 MBC levels of nitroimidazole compounds against gram-negative bacteria in this study; *E. coli* S: *Escherichia coli* ATCC25922, *K. pneumonia* S: *Klebsiella pneumonia* ATCC13883, CP-*E. coli*: carbapenemase producer *E. coli*, CP-*K. pneumonia*: carbapenemase producer *K. pneumonia*. Accordingly, compound **8g** had significantly higher bactericidal effects than metronidazole against standard strain and CP-*E. coli* ($p < 0.0001$)

while compounds **8j**, **8l**, **8m**, **8n**, and **8o** outperformed metronidazole against *K. pneumonia.*

Anti-biofilm effects

The biofilm formation by the isolates without exposure to the compounds has been exhibited in Table 6. Accordingly, the mean OD_{490} value of the six control wells included 0.05. None of the isolates were strong biofilm producers. Seven clinical *E. coli*, both of the clinical *K. pneumonia,* and MSSA and MRSA isolates were moderate biofilm producers. One *E. coli* isolate was weak biofilm producer and eight of them were biofilm non-producers. Furthermore, the biofilm formation of those isolates treated with the synthetic compounds has been

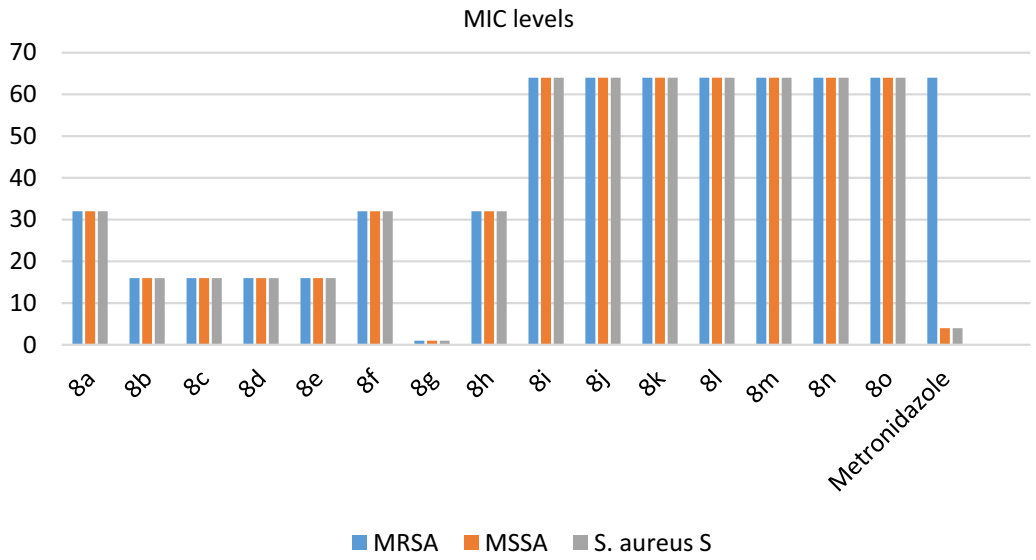

Fig. 4 MIC levels of nitroimidazole compounds against gram-positive bacteria in this study. Compound **8g** exhibited significantly higher antibacterial effects against MSSA and compounds **8b** ($p < 0.001$), **8c** ($p < 0.001$), **8d** ($p < 0.001$), **8e** ($p < 0.001$) and **8g** ($p < 0.0001$) exerted significantly higher antibacterial effects than metronidazole against MRSA. MRSA: methicillin-resistant *Staphylococcus aureus*, MSSA: methicillin-susceptible *Staphylococcus aureus*, NC: negative control

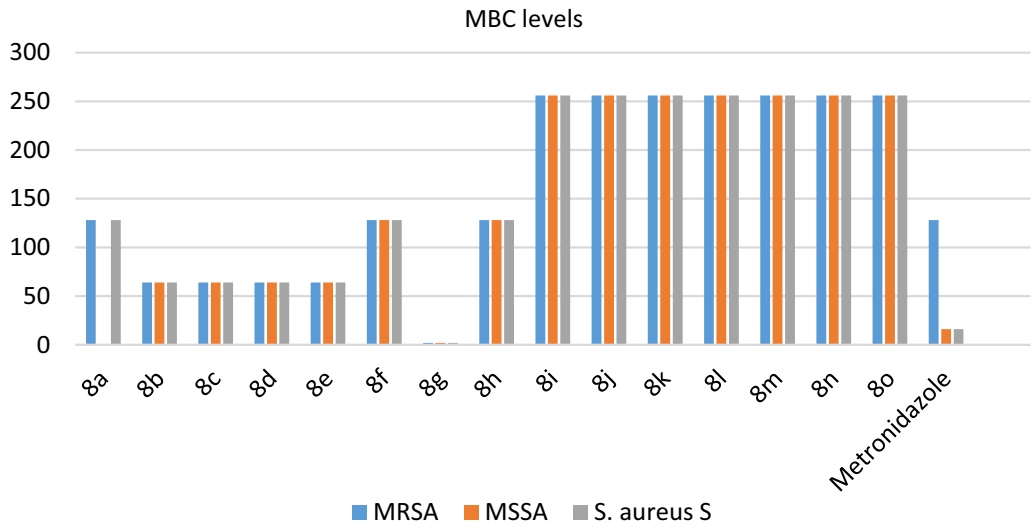

Fig. 5 MBC levels of nitroimidazole compounds against gram-positive bacteria in this study; MRSA: methicillin-resistant *Staphylococcus* aureus, MSSA: methicillin-susceptible *Staphylococcus aureus*

represented in Table 6. Accordingly, compounds **8c**, **8f**, **8g**, **8i**, **8n** and **8o** exhibited significant more potent anti-biofilm effects against clinical isolates. Moreover, moderate biofilm-producing *E. coli* isolates with higher OD values including E4, E10, E11 and E13 were able to produce biofilm when treated with compounds **8d**, **8h**, **8j** and **8l**. In addition, *K. pneumonia* K1 produced moderate biofilm in exposure to compounds **8b**, **8d**, **8j** and **8l**. MSSA biofilm formation was inhibited by all the compounds, while MRSA produced moderate biofilm in exposure to compounds **8i**-**8o** (Table 7).

The in silico analyses

Molecular dynamics simulation

The Root Mean Square Deviation (RMSD) values were calculated for both PBP2a and its ligands in the complex state to track the movement of Cα and heavy atoms in the protein and ligand during MD simulation. The

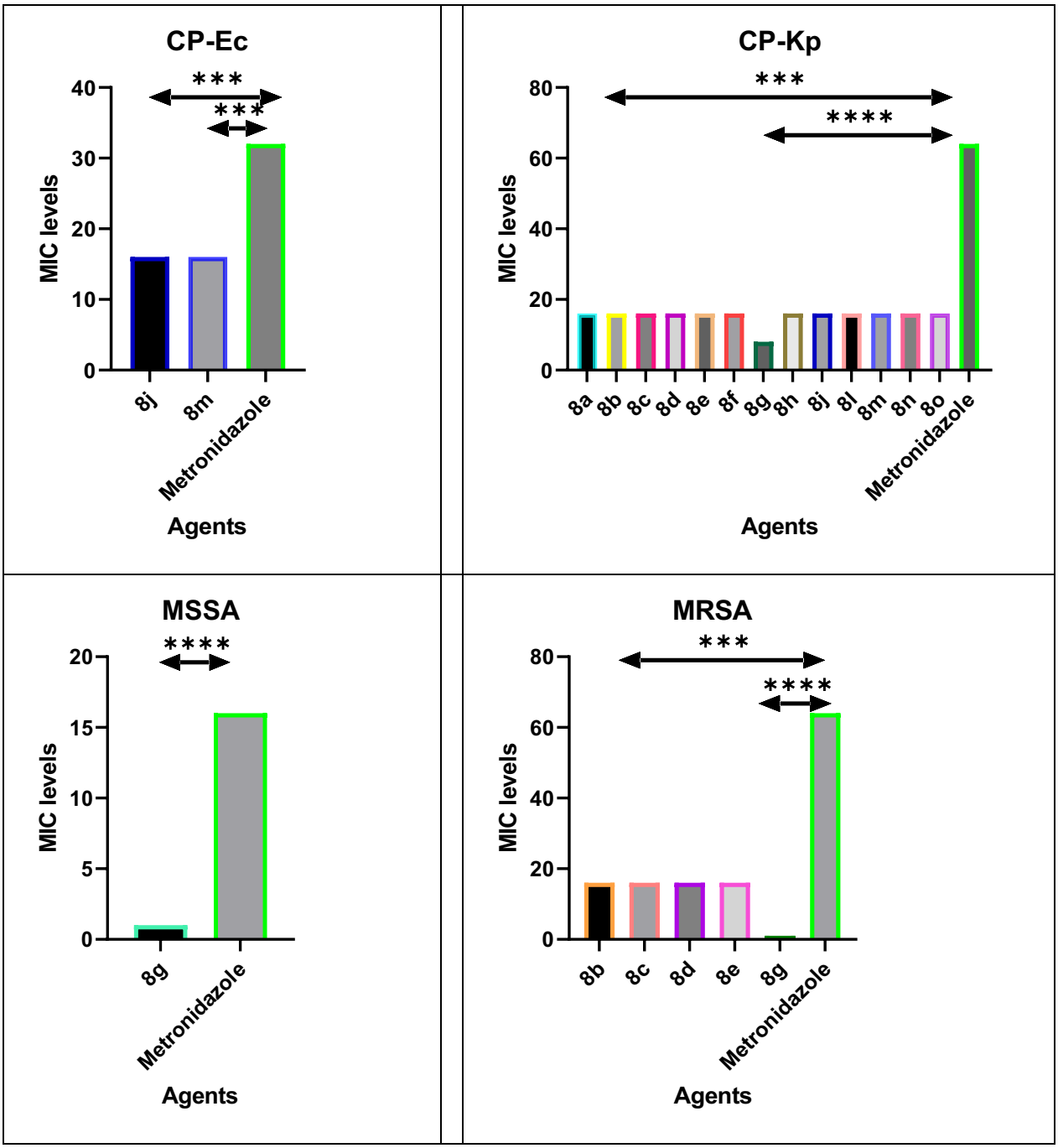

Fig. 6 The most potential antibacterial agents in this study with significant difference compared to metronidazole; CP-*E. coli*: carbapenemase producer *E. coli*, CP-*K. pneumonia*: carbapenemase producer *K. pneumonia*, MRSA: methicillin-resistant *Staphylococcus aureus*, MSSA: methicillin-susceptible *Staphylococcus aureus*

RMSD graph of PBP2a structure inferred consistent fluctuation throughout the simulation, with mean values of (0.34 ± 0.02) nm for metronidazole and (0.32 ± 0.02) nm for compound **8g**, indicating the stability of PBP2a during simulation (Fig. 7A). Additionally, Root Mean Square Fluctuation (RMSF) values of PBP2a in the complex state were calculated to analyze local structural fluctuations, with high values observed in loop regions of the protein. This high flexibility had no negative impact neither on the ligand binding nor the overall stability of the

Table 6 The biofilm formation by untreated bacterial isolates in this study

Isolate	Mean OD	NT Biofilm level
NC	0.05	Non-producer
PC	1.8	Strong
E1	0.071	Non-producer
E2	0.069	Non-producer
E3	0.060	Non-producer
E4	0.114	Moderate
E5	0.083	Weak
E6	0.059	Non-producer
E7	0.094	Moderate
E8	0.085	Moderate
E9	0.076	Non-producer
E10	0.167	Moderate
E11	0.122	Moderate
E12	0.061	Non-producer
E13	0.112	Moderate
E14	0.076	Non-producer
E15	0.084	Moderate
K1	0.138	Moderate
K2	0.091	Moderate
MSSA	0.118	Moderate
MRSA	0.099	Moderate

OD: optical density, NT: non-treated, E: *E. coli*, K: *K. pneumonia,* MSSA: methicillin-susceptible *S. aureus*, MRSA: methicillin-resistant *S. aureus*

PBP2a-ligand complexes, as shown in the RMSF plot which demonstrated consistent behavior of the PBP2a backbone in the presence of different ligands (Fig. 7B). For compounds at the catalytic site, RMSD values of 0.08 nm for metronidazole and 0.15 nm for compound **8g** indicated their proper interactions to the catalytic site and suitable stability in complex structures. Notably, compound **8g** exhibited higher flexibility compared to metronidazole, allowing for better exposure to catalytic site residues and facilitating interactions between residue side chains and the compound.

Binding mode and free binding energy analyses

During MD simulations, the values of ΔG_{bind}, van der Waals energy (ΔE_{vdw}), and electrostatic energy (ΔE_{ele}) components for complexes were obtained and are presented in Table 8. The MMPBSA method was employed to calculate the binding free energy and evaluate the energetic interactions of each compound with the binding landscape. For the complexes with metronidazole and compound **8g**, the computed binding free energies were determined to be −43.06 and −75.16 kJ/mol, respectively. The range of van der Waals contributions (ΔE_{vdw}) for the complexes varied from −161.28 to −84.12 kJ/mol, while the electrostatic contributions (ΔE_{ele}) for both ligands were approximately −29.50 kJ/mol. The analysis of the free energy components indicated that ΔE_{vdw} and ΔE_{ele} in the gas phase played a significant role in compound binding in the two complexes. On the other hand, solvation energies (ΔG_{GB}) had a negative impact on the binding energies. The study demonstrated that hydrophobic or nonpolar interactions ($\Delta E_{nonpolar}$) were the primary driving force behind compound binding, while polar interactions (ΔE_{polar}) were unfavorable for binding at the PBP2a binding site, with contributions ranging from 50.00 to 105.45 kJ/mol. Compound **8g** exhibited a lower ΔG_{bind} compared to metronidazole, suggesting the establishment of strong contacts with binding pocket residues. These findings have significant implications for the rational design of potential therapeutic agents targeting PBP2a. The identification of compound **8g** with superior binding affinities compared to the reference ligand opens up new possibilities for drug development. The detailed analysis of conformational stability, residue fluctuations, and binding energetics provides a solid framework for optimizing this compound and understanding its interactions with the target protein (Fig. 8).

The ADMET properties of potential candidate compound **8g** has been represented in supplementary Table 9.

ADMET properties of 8g	Status
Molecular weight	338.411
Number of hydrogen bond acceptors	5
Number of hydrogen bond donors	0
Number of rotational bonds	4
Partition coefficient in oil to water (CLogP)	1.21
Topological polar surface area(Å^2)	66.88
Aqueous solubility descriptor(LogS)	−3.00
Absorption	
Caco-2 cell permeability	0.796
Human intestinal absorption (HIA%)	92.383
Skin Permeability	−2.737
P-glycoprotein substrate	Yes
P-glycoprotein I inhibitor	Yes
P-glycoprotein II inhibitor	No
Distribution	
Volume of distribution	0.594
Barrier blood–brain permeability	−0.198
Central nervous system permeability	−1.987
Metabolism	
Cytochrome P450 1A2 inhibition	No
Cytochrome P450 2C19 inhibition	Yes
Cytochrome P450 2C9 inhibition	No
Cytochrome P450 2D6 inhibition	Yes
Cytochrome P450 2D6 substrate	No

Table 7 Biofilm formation levels by treated isolates

Isolate	8a	8b	8c	8d	8e	8f	8g	8h	8i	8j	8k	8l	8m	8n	8o
NC	N	N	N	N	N	N	N	N	N	N	N	N	N	N	N
PC	S	S	S	S	S	S	S	S	S	S	S	S	S	S	S
E1	N	N	N	N	N	N	N	N	N	M	N	M	N	N	N
E2	N	N	N	M	N	N	N	N	N	N	N	N	N	N	N
E3	N	N	N	N	M	N	N	N	N	N	N	N	N	N	N
E4	M	N	N	N	N	N	N	M	N	M	N	M	N	N	N
E5	N	N	N	N	N	N	N	N	N	N	N	N	N	N	N
E6	N	N	N	N	N	N	N	N	N	N	N	N	N	N	N
E7	N	N	N	M	N	N	N	N	N	N	N	N	N	N	N
E8	N	N	N	N	N	N	N	N	N	N	N	M	N	N	N
E9	N	N	N	N	N	N	N	N	N	N	N	N	N	N	N
E10	N	N	N	M	N	N	N	M	N	M	N	N	N	N	N
E11	N	N	N	N	N	N	N	N	N	M	N	M	N	N	N
E12	N	N	N	N	N	N	N	N	N	N	N	N	N	N	N
E13	N	N	N	M	N	N	N	M	N	N	N	N	N	N	N
E14	N	N	N	N	N	N	N	N	N	N	N	N	N	N	N
E15	N	N	N	N	N	N	N	N	N	N	N	N	N	N	N
K1	N	M	N	M	N	N	N	N	N	M	N	M	N	N	N
K2	N	N	N	N	N	N	N	N	N	N	N	N	N	N	N
MSSA	N	N	N	N	N	N	N	N	N	N	N	N	N	N	N
MRSA	N	N	N	N	N	N	N	N	M	M	M	M	M	M	M

E: *E. coli*, K: *K. pneumonia,* MSSA: methicillin-susceptible *S. aureus*, MRSA: methicillin-resistant *S. aureus*, NC: negative control, PC: positive control (biofilm producer *S. aureus*), S, N and M: strong, non-producer and moderate biofilm producer, respectively

ADMET properties of 8g	Status
Cytochrome P450 3A4 inhibition	No
Cytochrome P450 3A4 substrate	Yes
Excretion	
Total renal clearance	0.418
Renal OCT2 substrate	Yes
Toxicity	
Human ether related gene_inhibition I	No
Oral rat acute toxicity (LD50)	2.134
Oral rat chronic toxicity (LOAEL)	1.539
Skin sensitization	No

Discussion

In this study, propargylamine compounds (8a–8o) were synthesized by the A3 coupling reaction of sample substrates in the presence of CDSCS. These compounds with alkynyl group have considerable potential in medicinal chemistry for drug discovery [61, 62]. The antibacterial effects of these compounds demonstrated that the lowest MIC/MBC levels corresponded to compound **8g** against standard *S. aureus* (1/2 µg/mL) and *K. pneumonia* (8/32 µg/mL) standard and clinical strains. The in silico analyses confirmed the strong and stable binding of the compound **8g** to the active site of PBP2a of MRSA. This was comparable to those of metronidazole being 32–128 µg/mL against *K. pneumonia* and 32–64 µg/mL against *S. aureus*. Additionally, *E. coli* (with higher susceptibility of standard strains) strains were more susceptible to compounds **8h**, **8k**, **8l**, **8n** and **8o** with lower MIC and MBC levels. Comparably, MIC levels of metronidazole against *E. coli* ranged 16–64 µg/mL. Moreover, standard strains of *K. pneumonia* were more susceptible to compounds **8b**–**8e**, **8j**, **8k** and **8o**. Compounds **8a**–**8e** exerted higher antibacterial effects against clinical *K. pneumonia* and *S. aureus*. Interestingly, compounds **8i**–**8o** conferred significant higher antibacterial effects against Gram-negative strains. Furthermore, there was no significant difference in MIC or MBC values between *S. aureus* standard strain and each of clinical MSSA/MRSA. A lead thiazole compound could inhibit the growth of MRSA at 1.3 µg/mL in vivo and was non-toxic at up to 20 µg/mL [63]. Another metronidazole-triazole hybrids have depicted anti-MRSA effects at 4 µg/mL which was decreased to 1 µg/mL in combination to oxacillin at 1:1 ratio [64]. In a study, a series of synthetic small molecules demonstrated the eradication of MRSA rapidly at low and non-toxic levels (MIC of 3.125–6.25 µg/ml) [65]. In a study, synthetic biphenylthiazoles MIC against MRSA included 0.39 to 25 µg/mL [66]. MHY1383 synthetic compound has

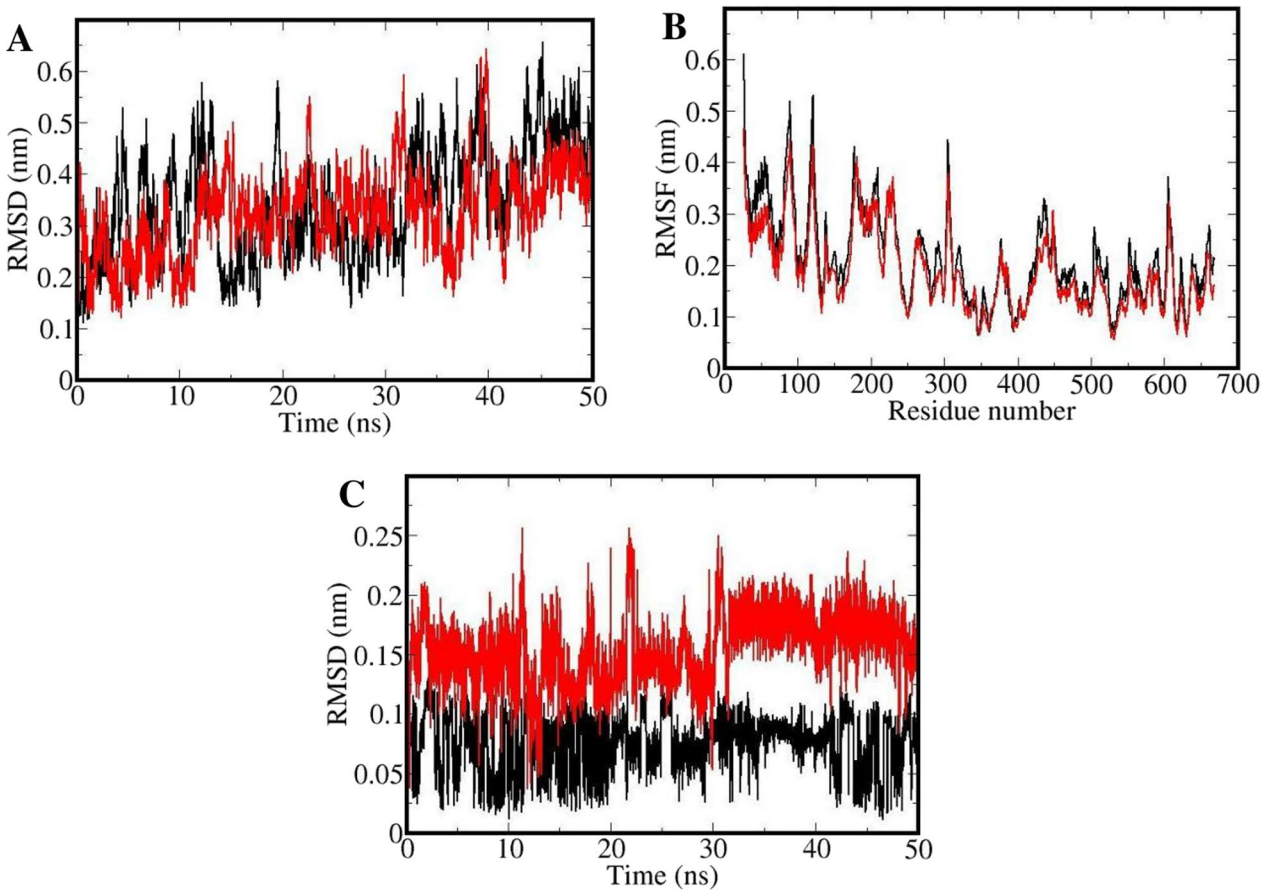

Fig. 7 **A** The RMSD of the Cα atoms changes during simulation time. **B** The RMSF of the Cα atoms along MD simulation. **C** The RMSD of the heavy atoms in the compound fluctuates during simulation time. The black and red colors are related to the PBP2a-metronidazole and PBP2a-compound **8g** complexes, respectively

Table 8 The contribution of various energy components in the ΔG_{bind} (kJ/mol)

	PBP2a-metronidazole	PBP2a-compound 8g
ΔE_{ele} [a]	−29.46 ± 3.53	−29.99 ± 3.04
ΔE_{vdW} [b]	−84.12 ± 3.84	−161.28 ± 2.47
ΔG_{PB} [c]	79.46 ± 6.25	135.44 ± 4.80
ΔG_{SA} [d]	−9.30 ± 0.15	−19.42 ± 0.31
$\Delta E_{non\text{-}polar}$ [e]	−93.42 ± 1.99	−180.7 ± 1.39
ΔE_{polar} [f]	50.00 ± 4.89	105.45 ± 3.92
ΔG_{bind}	−43.42 ± 3.44	−75.25 ± 2.78

[a] Electrostatic connection, [b]van der Waals connection, [c]Polar contribution of the solvation effect, [d]Non-polar contribution of solvation effect, [e] $\Delta E_{non\text{-}polar} = \Delta E_{vdW} + \Delta G_{SA}$, [f] $\Delta E_{polar} = \Delta E_{ele} + \Delta G_{GB}$

inferred antibacterial and anti-biofilm effects at low concentrations against *P. aeruginosa*, *E. coli*, *Bacillus subtilis* and *S. aureus* respectively at 1–10 pM, 1 pM, 1 nM, and 10 nM [67]. Pyrazole and Diene dione (Q1, M3 and Q7) compounds have deciphered antibacterial effects against *Enterococcus faecalis*, *Proteus mirabilis* and *S. aureus* at 0.312 mg/mL, 1.25 mg/mL and 0.156 mg/mL, respectively [68]. In this study, compound **8g** exhibited substantially low MIC and MBC levels against MSSA, MRSA and CR-*K. pneumonia* isolates. One aspect of selection of a proper antibacterial compound includes the evaluation of non-toxicity on normal cells. Some of studies have the limitation in this regard. We previously determined these compounds inhibitory effects against anaerobic parasite giardiasis which interacted to the DNA [44]. Indeed, nitro group of imidazole-based drugs can interact with biological nucleophiles (amino acids, nucleic acids and enzymes) and membrane permeabilization affecting multiple aspects of bacterial cell growth and function [64, 69]. Herein, the binding ability of compound **8g** to PBP2a was determined in silico which highlights cell wall synthesis inhibition, whereas its binding ability to the DNA is inevitable. Our synthetic compounds have three classes including Morpholine, Piperazine and Phenylpiperazine moieties with

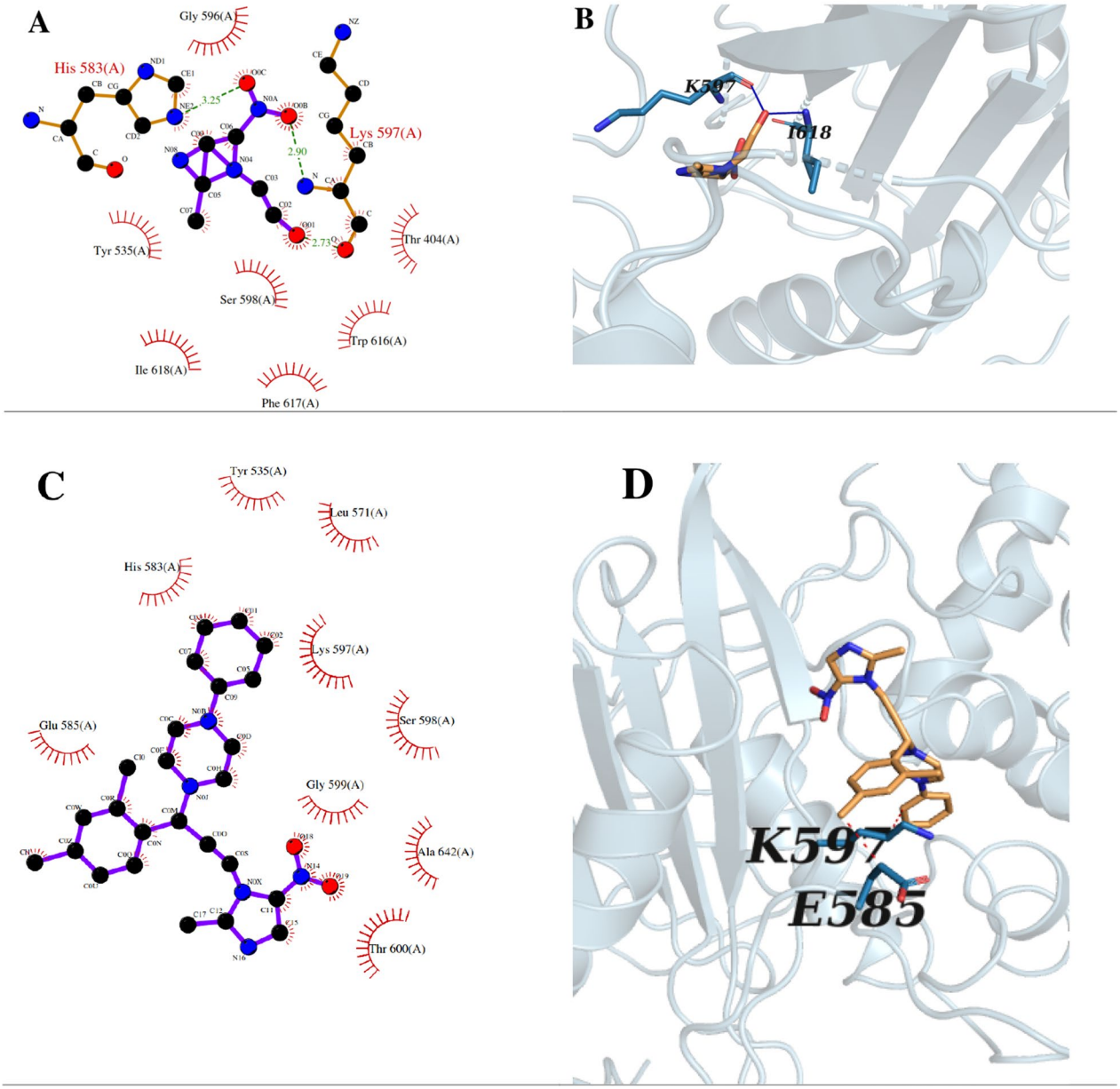

Fig. 8 The PBP2a complex was studied using MD simulations to generate 2D and 3D zoom views. The complex included metronidazole (**A** and **B**) and compound **8g** (**C** and **D**) as ligands. In the representation, PBP2a is shown as a light blue cartoon, with highlighted residues depicted as blue sticks. The ligands are shown as slate and wheat sticks. Hydrogen bonds are indicated by green dashed and blue lines, while red dots signify hydrophobic interactions. Spoked arcs illustrate nonbonded contacts between PBP2a residues and the ligands

potent antibacterial activity. Morpholine derivatives have exerted low cytotoxicity (10 μM) against WI-38 normal fibroblast cells [70, 71]. Moreover, Piperazine derivatives have inferred low cytotoxicity on human normal cells [72, 73]. Similar results have been demonstrated regarding Phenylpiperazine derivatives with low cytotoxicity against normal cells [74–76]. The considerable limitations of our study also included low number of drug-resistant bacterial isolates and lack of in vivo study and evaluation of molecular mechanisms underlying the bacterial killing by these novel compounds. Future studies can focus on these limitations and assessment of combination therapy to lower the costs, antibiotic resistance and side effects [77, 78].

Conclusion

Our study revealed that the nitroimidazole compounds **8a–8o** exerted disparate antibacterial and anti-biofilm effects, most potent of which was compound **8g** with lowest MIC and MBC levels against MSSA, MRSA and *K. pneumonia*. The findings were acceptable compared to the MIC and MBC levels of the reference antibiotic. Additionally, the in silico analyses confirmed the strong and stable binding of the compound **8g** to the active site of PBP2a of MRSA. Considering the promising inhibitory and killing effects of these synthesized compounds against drug-resistant bacterial pathogens, further assessments is warranted to verify their properties in vivo and clinical trials and their synergistic effects with antibiotics in future.

Supplementary Information

The online version contains supplementary material available at https://doi.org/10.1186/s13065-024-01333-w.

Supplementary Material 1.

Supplementary Material 2.

Acknowledgements
Not applicable.

Author contributions
E.Z. and A.G. conceptualized the study. E. Z. E. B. R. K. M. M. S.B. A.G. M.N.S.R. wrote the draft. E. Z. S.B, A. G. M.N. and S.R. performed the work. E.B. performed the in silico analyses. All authors reviewed the study.

Funding
This study was supported by Noncommunicable Diseases Research Center, Fasa University of Medical Sciences [Ethical code: IR.FUMS.REC.1402.057].

Data availability
Data is provided within the manuscript or supplementary information files.

Declarations

Consent for publication
All authors give consent for the publication of the manuscript in the Journal of BMC Chemistry.

Competing interests
The authors declare no competing interests.

Author details
[1]Noncommunicable Diseases Research Center, Fasa University of Medical Sciences, Fasa, Iran. [2]School of Advanced Technologies in Medicine, Fasa University of Medical Sciences, Fasa, Iran. [3]Department of Chemistry, Shiraz University of Technology, Shiraz 71555-313, Iran.

Received: 1 September 2024 Accepted: 29 October 2024
Published online: 18 December 2024

References

1. Huemer M, et al. Antibiotic resistance and persistence-Implications for human health and treatment perspectives. EMBO Rep. 2020;21(12): e51034.
2. Habboush Y, Guzman N. Antibiotic resistance. In StatPearls. 2023, StatPearls Publishing Copyright © 2023, StatPearls Publishing LLC.: Treasure Island (FL).
3. Logan LK, Weinstein RA. The epidemiology of carbapenem-resistant Enterobacteriaceae: the impact and evolution of a global menace. J Infect Dis. 2017;215(suppl_1):S28–36.
4. Ghasemian A, et al. Expression of adhesin genes and biofilm formation among *Klebsiella oxytoca* clinical isolates from patients with antibiotic-associated haemorrhagic colitis. J Med Microbiol. 2019;68(7):978–85.
5. Ghasemian A, et al. Report of plasmid-mediated colistin resistance in *Klebsiella oxytoca* from Iran. Rev Res Med Microbiol. 2018;29(2):59–63.
6. Aslam B, et al. Antibiotic resistance: one health one world outlook. Front Cell Infect Microbiol. 2021;11: 771510.
7. Morehead MS, Scarbrough C. Emergence of global antibiotic resistance. Prim Care. 2018;45(3):467–84.
8. Medina E, Pieper DH. Tackling threats and future problems of multidrug-resistant bacteria. Curr Top Microbiol Immunol. 2016;398:3–33.
9. Machowska A, StålsbyLundborg C. Drivers of irrational use of antibiotics in Europe. Int J Environ Res Public Health. 2018;16(1):27.
10. Wong SY, Tan BH. Megatrends in infectious diseases: the next 10 to 15 years. Ann Acad Med Singap. 2019;48(6):188–94.
11. Shanmugakani RK, et al. Current state of the art in rapid diagnostics for antimicrobial resistance. Lab Chip. 2020;20(15):2607–25.
12. Lesho EP, Laguio-Vila M. The slow-motion catastrophe of antimicrobial resistance and practical interventions for all prescribers. Mayo Clin Proc. 2019;94(6):1040–7.
13. Hermsen ED, et al. The role of the private sector in advancing antimicrobial stewardship: recommendations from the global chief medical officers' network. Popul Health Manag. 2021;24(2):231–40.
14. Ghafourian S, et al. Extended spectrum beta-lactamases: definition, classification and epidemiology. Curr Issues Mol Biol. 2015;17:11–21.
15. Tamma PD, et al. Infectious Diseases Society of America Guidance on the Treatment of Extended-Spectrum β-lactamase Producing Enterobacterales (ESBL-E), Carbapenem-Resistant Enterobacterales (CRE), and *Pseudomonas aeruginosa* with Difficult-to-Treat Resistance (DTR-*P. aeruginosa*). Clin Infect Dis. 2021;72(7):e169–83.
16. Bush K, Bradford PA. Epidemiology of β-lactamase-producing pathogens. Clin Microbiol Rev. 2020;33(2): e00047.
17. Peirano G, Pitout JDD. Extended-spectrum β-lactamase-producing enterobacteriaceae: update on molecular epidemiology and treatment options. Drugs. 2019;79(14):1529–41.
18. Saravanan M, Ramachandran B, Barabadi H. The prevalence and drug resistance pattern of extended spectrum β-lactamases (ESBLs) producing Enterobacteriaceae in Africa. Microb Pathog. 2018;114:180–92.
19. Doi Y. Treatment options for carbapenem-resistant gram-negative bacterial infections. Clin Infect Dis. 2019;69(Suppl 7):S565-s575.
20. Tamma PD, et al. Infectious Diseases Society of America 2022 Guidance on the Treatment of Extended-Spectrum β-lactamase producing Enterobacterales (ESBL-E), Carbapenem-Resistant Enterobacterales (CRE), and *Pseudomonas aeruginosa* with Difficult-to-Treat Resistance (DTR-*P. aeruginosa*). Clin Infect Dis. 2022;75(2):187–212.
21. Jean SS, Harnod D, Hsueh PR. Global threat of carbapenem-resistant gram-negative bacteria. Front Cell Infect Microbiol. 2022;12: 823684.
22. Sivaramakrishnan A, et al. Epidemiology and control measures of an OXA-48-producing Enterobacteriaceae hospital outbreak. Infect Prev Pract. 2020;2(3): 100021.
23. Hilliquin D, Lomont A, Zahar JR. Cohorting for preventing the nosocomial spread of carbapenemase-producing enterobacterales, in non-epidemic settings: is it mandatory? J Hosp Infect. 2020;105:534–45.
24. Katayama Y, Zhang HZ, Chambers HF. PBP 2a mutations producing very-high-level resistance to beta-lactams. Antimicrob Agents Chemother. 2004;48(2):453–9.
25. Argudín MA, et al. Epidemiology of the *Staphylococcus aureus* CA-MRSA USA300 in Belgium. Eur J Clin Microbiol Infect Dis. 2021;40(11):2335–47.
26. Tkadlec J, et al. The molecular epidemiology of methicillin-resistant *Staphylococcus aureus* (MRSA) in the Czech Republic. J Antimicrob Chemother. 2021;76(1):55–64.
27. Kaku N, et al. Changing molecular epidemiology and characteristics of MRSA isolated from bloodstream infections: nationwide surveillance in Japan in 2019. J Antimicrob Chemother. 2022;77(8):2130–41.

28. Hetem DJ, et al. Molecular epidemiology of MRSA in 13 ICUs from eight European countries. J Antimicrob Chemother. 2016;71(1):45–52.
29. Arshadi S, et al. N-Propargylamines: versatile building blocks in the construction of thiazole cores. Beilstein J Org Chem. 2017;13(1):625–38.
30. Raether W, Hänel H. Nitroheterocyclic drugs with broad spectrum activity. Parasitol Res. 2003;90:S19–39.
31. Varshney V, et al. Synthesis of nitroimidazole derived oxazolidinones as antibacterial agents. Eur J Med Chem. 2010;45(2):661–6.
32. Lemilemu F, et al. Synthesis, antibacterial and antioxidant activities of Thiazole-based Schiff base derivatives: a combined experimental and computational study. BMC Chem. 2021;15(1):67.
33. Marinescu M, et al. Synthesis, density functional theory study and in vitro antimicrobial evaluation of new benzimidazole Mannich bases. BMC Chem. 2020;14(1):45.
34. Zhu L, et al. Design, synthesis, and biological activity of novel 1,2,4-oxadiazole derivatives. BMC Chem. 2020;14(1):68.
35. Siwach A, Verma PK. Synthesis and therapeutic potential of imidazole containing compounds. BMC Chem. 2021;15(1):12.
36. Maeda K. A new antibiotic, azomycin. J Antibiot. 1953;6:182.
37. Anderson R, et al. Antibacterial agents: chemistry, mode of action, mechanisms of resistance and clinical applications. Amsterdam: John Wiley & Sons; 2012.
38. Patel OP, et al. Metronidazole-conjugates: a comprehensive review of recent developments towards synthesis and medicinal perspective. Eur J Med Chem. 2021;210: 112994.
39. Kannigadu C, N'Da D. Recent advances in nitroaromatics: the synthesis and development of anti-infective drugs. Curr Pharm Design. 2020;26:4658–74.
40. Nepali K, Lee H-Y, Liou J-P. Nitro-group-containing drugs. J Med Chem. 2018;62(6):2851–93.
41. Günay NS, et al. 5-Nitroimidazole derivatives as possible antibacterial and antifungal agents. Il Farmaco. 1999;54(11–12):826–31.
42. Rad MNS, et al. Copper-doped silica cuprous sulfate (CDSCS) as a highly efficient and new heterogeneous nano catalyst for [3+ 2] Huisgen cycloaddition. Tetrahedron. 2012;68(38):7812–21.
43. Soltani Rad MN, et al. Silica-tethered cuprous acetophenone thiosemicarbazone (STCATSC) as a novel hybrid nano-catalyst for highly efficient synthesis of new 1, 2, 3-triazolyl-based metronidazole hybrid analogues having potent antigiardial activity. Appl Organomet Chem. 2019;33(4): e4799.
44. Behrouz S, et al. Design, synthesis, antigiardial and in silico assessments of novel propargylamines containing nitroimidazole core. Tetrahedron. 2022;124: 133007.
45. Lewis I, James S. Performance standards for antimicrobial susceptibility testing. 2022.
46. Solgi H, et al. A comparative evaluation of five phenotypic methods for identification of carbapenemase-producing Enterobacteriaceae: a modified carbapenemase detection test. Microbiol Spectr. 2024;12:e00386-e424.
47. CLSI P. Standards for Antimicrobial Susceptibility Testing, In 33 ed. 2023, Clinical and Laboratory Standards Institute.
48. Trott O, Olson AJ. AutoDock Vina: improving the speed and accuracy of docking with a new scoring function, efficient optimization, and multithreading. J Comput Chem. 2010;31(2):455–61.
49. Abraham MJ, et al. GROMACS: high performance molecular simulations through multi-level parallelism from laptops to supercomputers. SoftwareX. 2015;1:19–25.
50. Hess B et al. On the importance of accurate algorithms for reliable molecular dynamics simulations. 2019.
51. Smith MD, et al. Force-field induced bias in the structure of Aβ21–30: a comparison of OPLS, AMBER, CHARMM, and GROMOS force fields. J Chem Inf Model. 2015;55(12):2587–95.
52. Mark P, Nilsson L. Structure and dynamics of the TIP3P, SPC, and SPC/E water models at 298 K. J Phys Chem A. 2001;105(43):9954–60.
53. Essmann U, et al. A smooth particle mesh Ewald method. J Chem Phys. 1995;103(19):8577–93.
54. Hess B, et al. LINCS: a linear constraint solver for molecular simulations. J Comput Chem. 1997;18(12):1463–72.
55. Kumari R, et al. g_mmpbsa-a GROMACS tool for high-throughput MM-PBSA calculations. J Chem Inf Model. 2014;54(7):1951–62.
56. Zhang Q, Ren H, Baker GL. An economical and safe procedure to synthesize 2-hydroxy-4-pentynoic acid: a precursor towards 'clickable' biodegradable polylactide. Beilstein J Org Chem. 2014;10(1):1365–71.
57. Barnett JA. The utilization of sugars by yeasts. Adv Carbohydr Chem Biochem. 1976;32:125–234.
58. Kleemann A et al. Pharmaceutical substances. 2011: Thieme New York, 2001.
59. Bourouina A, Meille V, de Bellefon C. About solid phase vs. liquid phase in Suzuki-Miyaura reaction. Catalysts. 2019;9(1):60.
60. Ghosh S, Biswas K. Metal-free multicomponent approach for the synthesis of propargylamine: a review. RSC Adv. 2021;11(4):2047–65.
61. Wang Y, et al. Asymmetric synthesis of syn-propargylamines and unsaturated β-amino acids under Brønsted base catalysis. Nat Commun. 2015;6(1):8544.
62. Zarenezhad E, et al. Immobilized [Cu(cdsalMeen)] on silica gel: a highly efficient heterogeneous catalyst for 'Click' [3 + 2] Huisgen cycloaddition. J Iran Chem Soc. 2017;14(2):509–19.
63. Mohammad H, Cushman M, Seleem MN. Antibacterial evaluation of synthetic thiazole compounds in vitro and in vivo in a methicillin-resistant *Staphylococcus aureus* (MRSA) skin infection mouse model. PLoS ONE. 2015;10(11): e0142321.
64. Negi B, et al. Anti-methicillin resistant *Staphylococcus aureus* activity, synergism with oxacillin and molecular docking studies of metronidazole-triazole hybrids. Eur J Med Chem. 2016;115:426–37.
65. Hamad M, et al. Antibacterial activity of small molecules which eradicate methicillin-resistant *Staphylococcus aureus* persisters. Front Microbiol. 2022;13: 823394.
66. Hagras M, et al. Investigating the antibacterial activity of biphenylthiazoles against methicillin- and vancomycin-resistant *Staphylococcus aureus* (MRSA and VRSA). J Med Chem. 2017;60(9):4074–85.
67. Hwang HJ, et al. Compounds that have an anti-biofilm effect against common bacteria at very low concentrations and their antibiotic combination effect. Antibiotics. 2023;12(5):853.
68. Rafiq MA, et al. Antibacterial, antibiofilm, and anti-quorum sensing potential of novel synthetic compounds against pathogenic bacteria isolated from chronic sinusitis patients. Dose Response. 2022;20(4):15593258221135732.
69. Li Z-Z, et al. Indole-nitroimidazole conjugates as efficient manipulators to decrease the genes expression of methicillin-resistant *Staphylococcus aureus*. Eur J Med Chem. 2019;179:723–35.
70. Jarrahpour A, et al. Synthesis of novel mono-and bis-Schiff bases of morpholine derivatives and the investigation of their antimalarial and antiproliferative activities. Med Chem Res. 2015;24:4105–12.
71. Rezaeivala M, et al. Some new morpholine-based Schiff-base complexes; synthesis, characterization, anticancer activities and theoretical studies. Inorg Chim Acta. 2020;513: 119935.
72. Ghasemi S, Sharifi S, Mojarrad JS. Design, synthesis and biological evaluation of novel piperazinone derivatives as cytotoxic agents. Adv Pharm Bull. 2020;10(3):423.
73. Liu M-C, et al. Synthesis and cytotoxicity of novel ursolic acid derivatives containing an acyl piperazine moiety. Eur J Med Chem. 2012;58:128–35.
74. Chen H, et al. Synthesis, biological evaluation and SAR of naftopidil-based arylpiperazine derivatives. Bioorg Med Chem Lett. 2018;28(9):1534–9.
75. Yurttaş L, et al. In vitro antitumor activity evaluation of some 1, 2, 4-triazine derivatives bearing piperazine amide moiety against breast cancer cells. Bioorg Med Chem. 2014;22(22):6313–23.
76. Sánchez-Céspedes J, et al. New 4-acyl-1-phenylaminocarbonyl-2-phenylpiperazine derivatives as potential inhibitors of adenovirus infection. Synthesis, biological evaluation, and structure–activity relationships. J Med Chemy. 2016;59(11):5432–48.
77. Alaoui Mdarhri H, et al. Alternatives therapeutic approaches to conventional antibiotics: advantages, limitations and potential application in medicine. Antibiotics. 2022;11(12):1826.
78. Siedentop B et al. The effect of combining antibiotics on resistance: a systematic review and meta-analysis. medRxiv. 2023.

Publisher's Note